Master's thesis

NTNU
Norwegian University of Science and Technology
Faculty of Information Technology and Electrical Engineering
Department of Engineering Cybernetics

Vebjørn Steinsholt

Developing New Abilities for Exoskeletons

Master's thesis in Cybernetics and Robotics
Supervisor: Anton Shiriaev
September 2022

NTNU
Norwegian University of
Science and Technology

Vebjørn Steinsholt

Developing New Abilities for Exoskeletons

Master's thesis in Cybernetics and Robotics
Supervisor: Anton Shiriaev
September 2022

Norwegian University of Science and Technology
Faculty of Information Technology and Electrical Engineering
Department of Engineering Cybernetics

NTNU
Norwegian University of
Science and Technology

Developing New Abilities for Exoskeletons

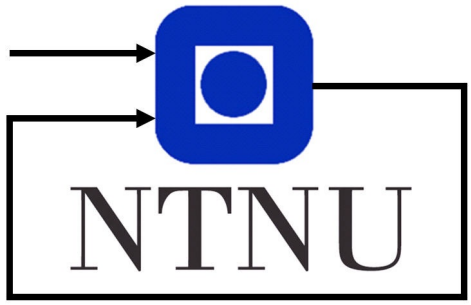

Author:
Vebjørn Steinsholt

Supervisor:
Anton Shiriaev

Master thesis
Department of Engineering Cybernetics
Norwegian University of Science and Technology
September 15, 2022

Summary

In this project it was attempted to find desirable trajectories for sit-down motions performed while wearing an exoskeleton and find a controller to stabilize these trajectories.
Due to a late change in experimental setup and unforeseen challenges in data processing and calculations this was unsuccessful. None the less the results are presented along with possible steps to improve on the experiment.

Preface

The work presented in this report is the result of work on TTK4900 - Engineering Cybernetics, Master Thesis, at The Norwegian University of Science and Technology. The purpose of the work is: To investigate desirable characteristics for exoskeletons for humans and implement controllers for this behaviour.

I would like to thank my supervisor Professor Anton Shiriaev for helping me and for his work in teaching several courses during my final 2 years of the master program. You have opened up new possibilities of knowledge.

Thank you to Sajid Rafique and Shaik Masud Rana for facilitating my visit to Gävle University, lending me their equipment and help. I would also like to thank my family, without your love and support I would not be able to do this

Vebjørn Steinsholt
Trondheim, September 15, 2022

Table of Contents

Summary i

Preface ii

List of Tables vii

List of Figures x

Abbreviations xi

Nomenclature xiii

1 Introduction 1
1.1 Motivation . . . 1

2 Scope 3
2.1 Tasks . . . 3
2.2 Structure . . . 3

3 Literature Review 5
3.1 Assistive robots/exoskeletons . . . 5
3.1.1 GE Hardiman . . . 5
3.1.2 Mihajlo Pupin Institute, exoskeletons . . . 6
3.1.3 Modular active orthosis - ”Active Suit” . . . 7
3.1.4 Hybrid Assistive Limb - HAL . . . 7
3.1.5 Berkeley Lower Extremity Exoskeleton (BLEEX) . . . 8
3.1.6 RoboKnee . . . 8
3.1.7 ATALANTE . . . 8
3.1.8 FB-AXO . . . 10
3.1.9 LegX (SuitX) . . . 11
3.1.10 Anthropomorphic and Non-anthropomorphic exoskeletons . . . 11
3.2 Underactuated systems and Orbital Stabilization . . . 12

4 Basic Theory **13**
4.1 Holonomic constraints . . . 13
4.2 Generalized Coordinates . . . 13
4.3 Euler-Lagrange Equation . . . 14
4.4 Fully Actuated and Underactuated systems . . . 16
4.5 Periodic systems and their properties . . . 17
4.5.1 Existence . . . 17
4.5.2 Orbital stability . . . 18
4.5.3 Moving Poincaré sections . . . 19
4.5.4 Transverse Coordinates . . . 20
4.6 Virtual Holonomic constraints (VHC) . . . 20
4.6.1 Reduced dynamics . . . 21
4.6.2 Periodic Solution . . . 22
4.6.3 Partial Feedback Linearization . . . 22
4.6.4 Transverse linearization . . . 25
4.6.5 Augmented system . . . 25
4.7 Stabilizing linear systems . . . 26
4.7.1 State Feedback Control . . . 26
4.7.2 Linear-quadratic Regulator . . . 27
4.8 Periodic Riccati differential equation . . . 27
4.8.1 Preliminaries . . . 28
4.8.2 Solving the periodic differential Riccati equation . . . 29

5 Experiment **31**
5.1 Hypothesis . . . 31
5.2 Experimental Setup . . . 31
5.2.1 Original Plan . . . 31
5.2.2 Revised plan . . . 31
5.3 Inertial Sensors . . . 33
5.3.1 Synchronization functions . . . 34

6 Analysis **37**
6.1 Results . . . 37
6.2 Sources of error . . . 39
6.2.1 Movement of sensor . . . 39
6.2.2 Time length of movement . . . 39
6.2.3 Number of sensors . . . 39
6.2.4 World frame orientation . . . 40
6.2.5 Magnetic Distortion . . . 40
6.3 Potential improvements . . . 41
6.3.1 World frame orientation . . . 41
6.3.2 Object orientation frame . . . 41
6.3.3 Using more sophisticated software . . . 42
6.3.4 Methods of obtaining joint angles by way of IMUs . . . 42

7 Conclusion **43**
7.1 Future work and continuation 43
7.1.1 Original Setup 43
7.1.2 Revised plan 44
7.1.3 Continuation 44

Bibliography **45**

A Theorems, definitions and lemmas **51**
A.1 Theorems 51
A.2 Lemmas 51
A.3 Definitions 51

B Proofs **53**
B.1 Proof of A.2.1 53
B.2 Proof of 4.6.1 53
B.3 Proof of 4.6.2 54
B.4 Proof of 4.7.1 55

C Specialization project report **57**

List of Tables

5.1 Test person measurements 33
5.2 Sensor heights, where h_0 us the height from the floor to the lowest part of the sensor and h_1 is the height from the floor to the top of the sensor . . . 34
5.3 Estimated masses, based on percentages of body weight for each limb of the male subject in [11].Estimated centers of mass, based on *Large male aviator* in [41] scaled up to the height of the test person. Since the trunk, lower leg and arm are made up of more than one segment the combined center of mass was calculated by $\vec{R} = \frac{1}{M}\sum_1^n m_i\vec{r}_i$ found in [9] 34

List of Figures

1.1 Early concept of an exoskeleton to augment walking, running and jumping 2

3.1 Hardiman I prototype, GENERAL ELECTRIC CO SCHENECTADY NY SPECIALTY MATERIALS HANDLING PRODUCTS OPERATION, Public domain, via Wikimedia Commons[12] 5
3.2 HAL-5 (Type-B) Reprinted by permission from Springer Nature Customer Service Centre GmbH: Springer, Berlin, Heidelberg, Robotics Research. Springer Tracts in Advanced Robotics, vol 66. [46], Copyright © 2014, Springer-Verlag Berlin Heidelberg 8
3.3 Concept sketch of Berkeley Lower Extremity Exoskeleton. When proper control action is used it cancels the weight of the payload from the user and eases the movement. © 2006 IEEE 9
3.4 Degrees of freedom and actuators of the Berkeley Lower Extremity Skeleton [69]© 2006 IEEE 9
3.5 RoboKnee design showing knee brace and Series Elastic Actuator, The joint position and velocity are deduced based on the actuator stroke and linear velocity, measured with a linear encoder. Not shown are the Velcro straps and the lower connection piece[40] © 2004 IEEE 10
3.6 Two exoskeletons from [3] with the same actuators. (a) is the non-anthropomorphic design and (b) is an anthropomorphic design. Copyright © 2014, IEEE . . 12

4.1 Unconstrained system of k particles with $3k$ degrees of freedom 14
4.2 Inner-loop/outer-loop structure 16
4.3 Illustration of Poincaré - Bendixson Criterion.Reprinted under Creative Commons License[55] 18
4.4 Moving Poincaré section for periodic trajectory $x^*(t)$. Reprinted from Annual Reviews in Control Vol.32, Issue 2, A.S. Shiriaev, L.B. Freidovich, I.R. Manchester , Can we make a robot ballerina perform a pirouette? Orbital stabilization of periodic motions of underactuated mechanical systems, Pages 200-211, Copyright ©(2008), with permission from Elsevier . 20

5.1 LB-AXO 32
5.2 The world(G) and sensor(S_i) frames on the test person. The MTw calculates the orientation between the sensor-fixed coordinate system, and an earth-fixed coordinate system, G. By default G is defined as: X positive when pointing to the local magnetic North. Y according to the right handed coordinates(West). Z positive when pointing up [63] 33

6.1 Euler Angles when the exoskeleton is not worn during the sitting motion. 38
6.2 Euler Angles when the exoskeleton is worn, but turned off during the sitting motion. 38
6.3 The pitch angle at the Thigh from the IMU sensors, without exoskeleton. Notice in particular the motion artifacts and the jump at $t \approx 1.5s$ 39
6.4 The pitch angle at the thigh from the IMU sensors, when the exoskeleton is worn and assistance is turned off. Notice in particular the motion artifacts and the jump at $t \approx 1.5s$ which is very similar to the case when the exoskeleton is worn 40
6.5 The data of Figure 6.4 smoothed with a Gaussian filter. This is monotonic, but one can't guarantee that this if fully representative of the movement itself. 40
6.6 Relation between Sensor frame(S) and Object frame(O) 41

Abbreviations

DoF	=	Degrees of freedom
VHC	=	Virtual Holonomic Constraints
LQR	=	Linear–quadratic regulator
PRDE	=	Periodic Ricatti Differential Equation
wrt	=	With regards to
i.e	=	*id est* = that is
EMG	=	Electromyographical
VHC	=	Virtual Holonomic Constraints
STS	=	Sit to stand
LMI	=	Linear matrix inequality

Nomenclature

Symbol		Definition
$\mathbb{R}^n$	=	The real coordinate space of dimension n
$\dot{\theta}$	=	$\frac{d\theta}{dt}$, time derivative of θ
$\ddot{\theta}$	=	$\frac{d^2\theta}{dt^2}$, time derivative of θ
v_i	=	Velocity of body i
$\frac{\partial}{\partial\theta}$	=	Partial derivative with regards to coordinate θ
u	=	Control input
w^T	=	The transpose of the matrix w
τ_i	=	torque applied at the i-th link
$\mathcal{K}$	=	Total kinetic energy of system
$\mathcal{P}$	=	Total potential energy of system
$\mathcal{L}$	=	Lagrangian
$\phi(\theta)$	=	Motion generator/Synchronization function
$\alpha\beta\gamma$-equation	=	$\alpha\ddot{\theta} + \beta(\theta)\dot{\theta}^2 + \gamma(\theta) = 0$
k_i	=	Coefficients of the polynomial chosen for $\phi(\theta)$
∇f	=	Gradient: grad f
$x_{i\perp}$	=	i-th transverse coordinate
I	=	Integral of motion
$K(t)$	=	LQR-gain for the input $v(t) = K(t)x_\perp(t)$ to the linearised system
Q	=	Weight on deviation from states in LQR-control
R	=	Weight on use of control action in LQR-control
$P(t) = P(t+T) = P(t)^T$, $\forall t \in [0, T]$	=	Solution of the periodic Ricatti equation

Term		Explanation
Coronal/frontal plane	=	The vertical plane dividing the body in two asymmetrical halves
Sagittal/longitudinal plane	=	The vertical plane dividing the body in two symmetrical halves
Myoelectric signal	=	Measurement of action potential of motor units when a muscle contracts. Aggregate of these signals is a measurement of the degree of muscle contraction in an area(After signal processing)[25].

1

Introduction

1.1 Motivation

> ”At bottom, robotics is about us. It is the discipline of emulating our lives, of wondering how we work.” - Rod Grupen [16]

”Exoskeletons”[from Greek exō, meaning out, outside [29] and skeleton, an artificial external supporting structure[30]] has been a staple of science fiction for almost a hundred years. The likely first conception of a exoskeleton was by Nicholas Yagn [65] seen in figure 1.1 this was an entirely passive skeleton in that it only used the energy of motion stored in springs to ease locomotion. To the knowledge of the author this exoskeleton was never implemented in practice, but this shows through the use of exoskeletons have been part of the human consciousness for a long time.

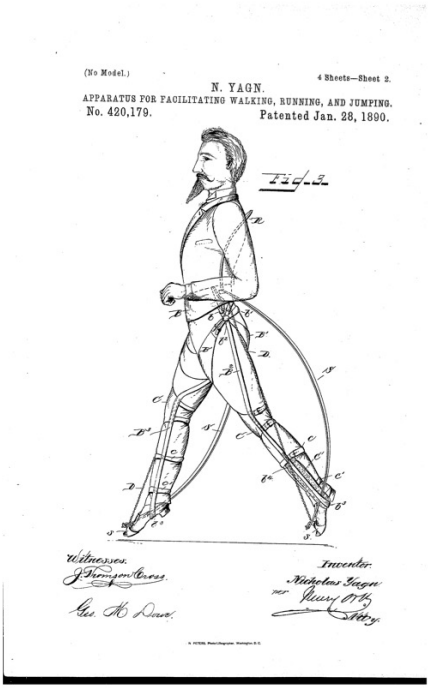

Figure 1.1: Early concept of an exoskeleton to augment walking, running and jumping

From this early beginning there have been taken great strides in the development of exoskeletons and they are no longer just science fiction. Especially in hardware the technology is proceeding at a great pace, but in the control systems they often rely on non-sophisticated methods. Usually the exoskeletons are controlled through state-control, impedance control or electromyographical (EMG) control, these methods have been shown to be usable in applications(this will be discussed further in the literature review in chapter 3) .

What will be attempted in here is making an exoskeleton move more like a human.This is done considering the nature and limitations our bodies have and using the method of Virtual Holonomic Constraints(VHC) and orbital stabilization of underactuated systems. A further benefit is that if one can manage to control a fully actuated exoskeleton($u_i \neq 0 \quad \forall \quad i = 1 \dots n$) by only applying control action on all but one of the joints($n - 1$), then that actuator may be redundant and can be removed reducing weight and most likely cost of the exoskeleton. Both of these are critical objectives for the mass adoption of these types of devices

2

Scope

2.1 Tasks

1. Perform a study on theory of underactuated systems and assisting exoskeleton technologies.
2. Investigate desirable characteristics of sit-down motions
3. Develop a control system for a human-exoskeleton system
4. Test the developed control system on a given exoskeleton setup.
5. Discuss further steps and improvements

2.2 Structure

First a literature review will be presented. Furthermore general theory will be reviewed, the results of the experiments will be shown and analysed before discussion and concluding remarks.

3

Literature Review

3.1 Assistive robots/exoskeletons

As mentioned in chapter 1 the earliest attempts in exoskeletons known to the author was by Nicholas Yagn in the late 19-th century.

3.1.1 GE Hardiman

In more modern times starting with General Electrics ”Hardiman I” worked on from 1965-1971[26]. This was an active exoskeleton that was powered by hydraulics and it had 30-degrees of freedom (DOF). The prototype weighed around 680 kg and as can be seen in figure 3.1 it was very bulky. These problems meant that it was never fully implemented, but lead to advances in power supplies and human-machine interfaces[6].

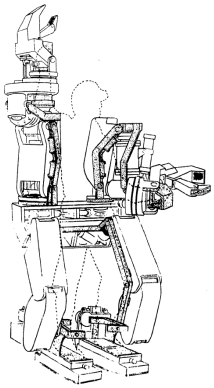

Figure 3.1: Hardiman I prototype, GENERAL ELECTRIC CO SCHENECTADY NY SPECIALTY MATERIALS HANDLING PRODUCTS OPERATION, Public domain, via Wikimedia Commons[12]

3.1.2 Mihajlo Pupin Institute, exoskeletons

A family of exoskeletons trace their origins to Mihajlo Pupin Institute in the late sixties early seventies. A short presentation of the will follow below

"Kinematic Walker"

In 1969 researchers at Mihajlo Pupin Institute in Belgrade developed the "kinematic walker". This exoskeleton was pneumatically powered and had 6 DoF(3 on each leg) where the knee and hip joints were actuated and the ankle joints was passive and only actuated in the "sagittal plane" [The vertical plane dividing the body in two symmetrical halves] . This exoskeleton was not very sophisticated, but in tests on healthy subjects imitating a limp state and only contributing in stability they were able to provide a shuffling gait[62, p. 321]. This exoskeleton was the first successful active exoskeleton developed [61].

"Partial" active exoskeleton

In 1970 the researchers further developed an active pneumatic exoskeleton. This model had three active DoF per leg and an additional actuated DoF for stabilizing by moving the body in the coronal plane [62, p. 321-322]. This exoskeleton was controlled by an electronic function generator. During trials fully paraplegic[paraplegia:partial or complete paralysis of the lower half of the body with involvement of both legs that is usually due to injury or disease of the spinal cord in the thoracic or lumbar region[31]] patients were able two walk when supported by a person on each side or using a rolling support structure. These limitations was due to instability from not being able to actuate the torso.

"Complete" exoskeleton

In the following year(1971) the problems with the "partial" active skeleton was resolved by adding a corset which allowed the torso to be actuated in bot the frontal and sagittal plane. This stabilisation allowed paraplegic patients to walk with crutches.

There was also added force feedback from the soles in the feet, where three force transducers were measuring the ground reaction force. The control system compensated and kept these forces inside a predetermined range further contributing in stabilising the system[62, p. 323-324]. This exoskeleton was pneumatically powered. It was later concluded that pneumatically driving the exoskeletons was not practical and the researchers moved on to electrical powered drives [62, p. 321-326]. This exoskeleton was realized and tested at Belgrade Orthopedic Clinic in 1972[61].

"Complete electrical" exoskeleton

Moving away from pneumatically powered exoskeletons to electrical ones were done in 1973 [62, p. 325-326] this was mainly due to practical concerns. These early efforts became a starting point for many other medical exoskeletons and lead to the development of Zero-Moment Point method[61] which has found great purchase on the field of humanoid robotics.

3.1.3 Modular active orthosis - ”Active Suit”

The ”active suit” was worked on between 1974-1978 [62, p. 326-330] and was made to help a wide range of patents with varying degrees of dysthrophy[any of various bodily disorders, characterized by wasting of tissues[10]]. These users have problems(of differing levels) with walking normally even without any challenging elevation or terrain. This is because of weakness in some neuro-muscular systems like hips and knees. The ”active suit” provides aid to the hip and knee joints to aid in the movement by using servomotors at these joints. The system was powered by a nickel-cadmium battery which weighed about 2 kilograms. This battery provided enough energy for 45 minutes of walking on level ground or climbing up the stairs to the third floor 2-3 times

The apparatus was controlled by the user through switches. For walking gaits there were three choices level ground, up stairs and down stairs. The motion is initiated by a stop-start switch, after initiation the user can control the motions pace, stride and direction by additional button commands.

The developers of the exoskeleton reported good results and further expanded upon the technology in 1980. This model improved on the control system, lightened the weight of the power supply and added an additional actuator at each knee.

3.1.4 Hybrid Assistive Limb - HAL

The Hybrid Assistive Limb(HAL) is a hybrid exoskeleton meaning that it is designed with multiple applications ind mind, like medical assistive device, heavy work load assistance among others[46]. The exoskeletons are made by the Japanese company Cyberdyne, lead by Yoshiyuki Sankai the principle lead of the development of the HAL-system. The development of the first version of the HAL began in 1992, in figure 3.2 HAL-5 type-B and in 2017 the Medical HAL(lower limb exoskeleton) received approval from the U.S. Food and Drug Administration(FDA)[37].

HAL utilizes a control system in two parts, analogous to the human body it has a voluntary and autonomous part.The voluntary system measures bioelectrical signals from the user and uses these signals to amplify the joint torque of the user. Myoelectric and other bioelectrical signals are measured just before the muscle contracts and can then be used to measure a users intention to move, stop or swing the leg . This means that the HAL’s voluntary control system can be used to augment healthy persons, but also patients with some lower limb handicaps, but obviously not in the case of significant injuries on the spinal column[56].

When the intent of the user is detected the control system attempts to achieve joint angles that corresponds to reference trajectories that are pre-recorded from a healthy person. These trajectories are separated into two gait phases, swing phase and support phase[67].

In the autonomous control system of the HAL exoskeleton reaction forces, shifts in the centre of gravity and joint angles are used to estimate the the intent of the user in order to support that movement[46]. For instance when a user shifts their weight from one leg to another that is an indication that they intend to take a step. This allowed a patient with partial paralysis on the left leg to walk only being able to limp with the aid of a cane in both hands before.

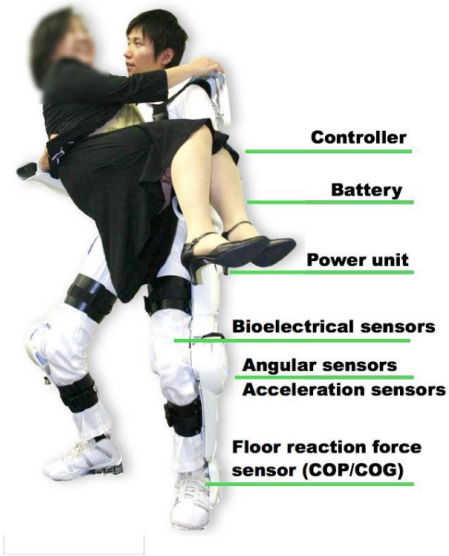

Figure 3.2: HAL-5 (Type-B) Reprinted by permission from Springer Nature Customer Service Centre GmbH: Springer, Berlin, Heidelberg, Robotics Research. Springer Tracts in Advanced Robotics, vol 66. [46], Copyright © 2014, Springer-Verlag Berlin Heidelberg

3.1.5 Berkeley Lower Extremity Exoskeleton (BLEEX)

In contrast to the previous mentioned exoskeletons Berkeley Lower Extremity Exoskeleton is not a medical exoskeleton, but a device to augment the strength of healthy persons. It is intended to carry it's own weight and a payload [70]. It has 7-degrees of freedom on each leg. 3 DOF at the hip, one DOF at the knee and 3 DOF at the hip. . It is fully actuated in the sagittal plane, meaning at one DOF at the hip, knee and ankle and one additional actuator at the hip(see figure 3.4). The exoskeleton allowed the users to move a payload of 75 kg at a walking speed of up to 1.3 m/s.

3.1.6 RoboKnee

The researchers behind the RoboKnee shows that one can enhance human performance without a complex design. It is a 1-DoF knee exoskeleton which augments the users strength and endurance. A linear series elastic actuator provided additional torque around the knee to aid the user [40] see figure 3.5.

A user was able to do one-legged knee bends with an additional weight of 60 kg without becoming tired having only to be able to do it 2-3 times without assistance.

3.1.7 ATALANTE

As shown in the early days of exoskeletons a challenge was achieving hands-free stable walking for paraplegics (section 3.1.2) the *ATALANTE*-exoskeleton made by Wander-

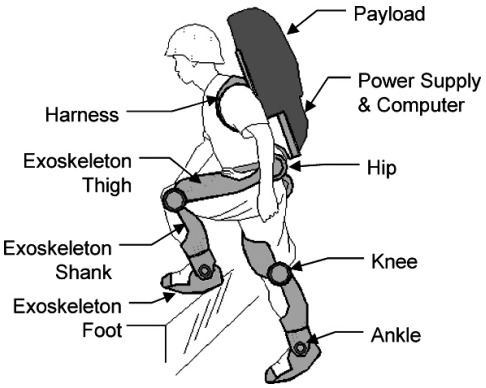

Figure 3.3: Concept sketch of Berkeley Lower Extremity Exoskeleton. When proper control action is used it cancels the weight of the payload from the user and eases the movement. © 2006 IEEE

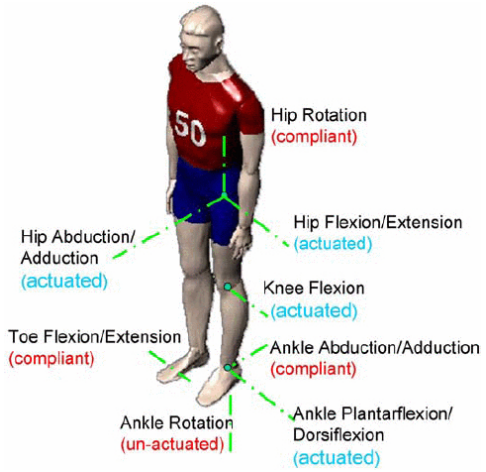

Figure 3.4: Degrees of freedom and actuators of the Berkeley Lower Extremity Skeleton [69]© 2006 IEEE

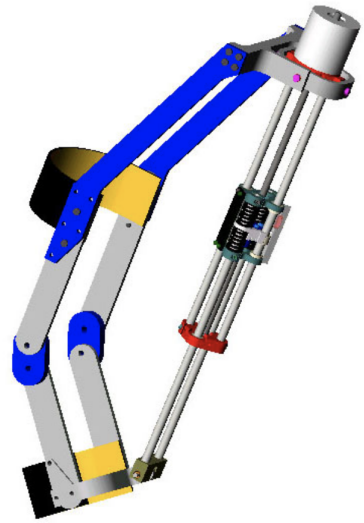

Figure 3.5: RoboKnee design showing knee brace and Series Elastic Actuator, The joint position and velocity are deduced based on the actuator stroke and linear velocity, measured with a linear encoder. Not shown are the Velcro straps and the lower connection piece[40] © 2004 IEEE

craft was the first exoskeleton to achieve dynamic hands-free walking for these patients [17][The ATALANTE along with REX from Rex Bionics [43] are the only known exoskeletons to manage this that are currently on the market[33, p. 123]]. The former authors achieve a robust feedback controller for this objective through virtual constraints, optimization and supervised machine learning. Further work mentioned is control algorithms that can deal with uncertainties in the model and sit-to-stand and stand-to-sit the former of which is addressed in [33].

The aforementioned authors develop control to achieve sit to stand motion(STS) for the ATALANTE. Interestingly they achieve this for a the full 3D lower-limb exoskeleton and not just in the sagittal plane. The utility of this is for instance a wheelchair bound patient being able to start from sitting in the wheelchair and transition into walking , this is essential because this can make the user self-dependent(if the exoskeleton can be put on in a sitting position).

3.1.8 FB-AXO

The FB-AXO suit is a full body(FB) exoskeleton comprised of an upper body(UB) and lower body(LB) module. In total there are 27 DoF, where 10 are active and 17 are passive respectively. Most relevant for this project is the lower body module. LB-AXO has 12-DoF where 4 are active and 8 are passive(6 on each leg) . It is primarily actuated at the hip and knee joints in the sagittal plane[8]. For control of the exoskeletons at least some of the models use Impedance-based force tracking control in the task space and Disturbance observer based dynamic load torque compensator in the joint space[27] The AXO-LB and

its predecessor[1] [1] the EXO-legs[60] are not intended for use by paraplegics and other users with severe injuries, but rather to enhance the movement of elderly persons to allow them to have an improved life in older age.

3.1.9 LegX (SuitX)

The LegX is a lower-body passive exoskeleton with two different operating modes, spring assist and locked mode [39]. When in the spring assist mode the exoskeleton stores the energy during the sit down motion and releases the energy when standing up. The level of support can be chosen between a high and a low level.

In Locked mode the exoskeleton supports a ”floating” seated/squatting position.

Being a passive exoskeleton it does not have any motors, and therefore no encoders to supply the joint angles of the exoskeleton-user system. This means that one must use other means to obtain these measurements. This will be further discussed in Chapters 5 and 6.

3.1.10 Anthropomorphic and Non-anthropomorphic exoskeletons

It might seem obvious that exoskeletons should be ”anthropomorphic”[... comes from the Late Latin word anthropomorphus, which itself traces to a Greek term birthed from the roots anthrōp- (meaning ”human being”) and -morphos (-morphous).[28], morphous: having (such) a form] meaning that the joints and links of the robot is close to the placement of the humans joints and limbs. Most exoskeletons are anthropomorphic to some degree, but this is not a hard constraint as shown in [3]. The authors relaxed these constraints and saw a improvement in dynamical performance compared to a similar anthropomorphic design(see figure 3.6) and this also made it possible to optimize the position of the masses on the exoskeleton, like moving the actuators closer to the torso.

[1] predecessor, in that both exoskeletons are part of the Active Assisted Living Program(AAL) [2]

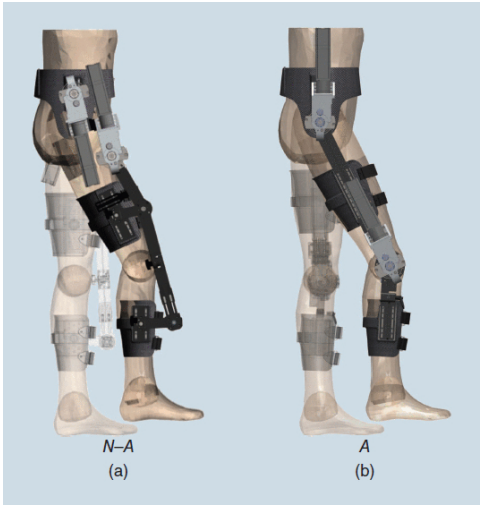

Figure 3.6: Two exoskeletons from [3] with the same actuators. (a) is the non-anthropomorphic design and (b) is an anthropomorphic design. Copyright © 2014, IEEE

3.2 Underactuated systems and Orbital Stabilization

Human motions like walking, sitting and rising motions are periodic and we are therefore interested stabilizing these motions orbitally or make a system without these oscillations oscillate in a similar way. Another concern is that humanoids are either weakly actuated or may have no actuation in some of the joints. This means that the old methods of orbital stabilization (OB) are not sufficient. In [51] the authors present a clear method of orbital stabilization of these system through Virtual Holonomic constraints.

In [32] extract desirable characteristics of humans from real human actors and use the methods of [51] to impose these virtual constraint onto a human robot model based anthropomorphic data. In [38] they use the method on a model of the robot Mahru III

In this thesis it was attempted to adapt these results to a exoskeleton designed for human use.

4

Basic Theory

4.1 Holonomic constraints

Constraints g_i, that can be written on the form:

$$g_i(r_1, \ldots, r_k, t) = 0 \quad i = 1, \ldots, l \tag{4.1}$$

are holonomic and nonholonomic otherwise [54].

4.2 Generalized Coordinates

If one considers a system of k particles with mass m_i and positions given by $\vec{r}_1 \ldots \vec{r}_k$ in a thee dimensional Cartesian coordinate system (see figure 4.1). If this system is unconstrained it has $3k$ degrees of freedom. The dynamics of each particle is then easily defined by Newton's second law:

$$\frac{d}{dt}(mv) = f \tag{4.2}$$

where m is the particle mass, v particle velocity and f is the sum of external forces acting on the particle. In our robotics applications mass is constant and one gets the familiar $ma = f, a = \frac{d}{dt}v$. On the other hand if the system is constrained in some way, one can no longer just consider the external forces, but must also account for the constraint forces that are needed to enforce the constraints. The benefit is that if the system is subjected to l holonomic constraints on the form of (4.1) the system may be described by n independent coordinates $q_1, \ldots q_n$ where $n = 3k - l$.

The position of the each particle, i, can then be written as:

$$\vec{r}_i(t) = \vec{r}_i(q_1, \ldots, q_n, t) \tag{4.3}$$

These n coordinates are the systems generalized coordinates $q = [q_1, \ldots, q_n] \in \mathbb{R}^n$. For n-link robot manipulator the joint variables form a set of generalized coordinates.

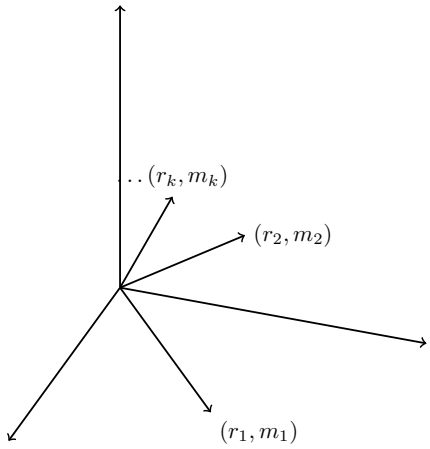

Figure 4.1: Unconstrained system of k particles with $3k$ degrees of freedom

4.3 Euler-Lagrange Equation

The Euler-Lagrange equation is a popular method to derive the dynamics of a system along with the Newton-Euler formulation. Euler-Lagrange equation can be derived by D'Alembert's principle, but these details are omitted for brevity; see for instance [54, p. 248-250]. The *Lagrangian* is defined as:

$$\mathcal{L}(q, \dot{q}) := \mathcal{K}(q, \dot{q}) - \mathcal{P}(q) \tag{4.4}$$

Where $\mathcal{K}$ is the kinetic energy of the system and $\mathcal{P}$ the potential energy. The kinetic energy is given by:

$$\mathcal{K} := \frac{1}{2}\dot{q}^T \left[\sum_{i=1}^{n} \left(m_i J_{v_i}(q)^T J_{v_i} + J_{\omega_i} R_i(q) I_i R_i(q)^T J_{\omega_i} \right) \right] \dot{q} = \frac{1}{2}\dot{q}^T D(q) \dot{q} \tag{4.5}$$

where D is the $n \times n$ symmetric, positive definite inertia matrix, m_i is the i-th link mass, J_{v_i} is the i-th link velocity jacobian, J_{ω_i} is the i-th link angular velocity jacobian, R_i is the rotation matrix from the world frame to the i-th body frame and I_i is the inertia tensor of the i-th link.

The potential energy is only dependent only on the generalized coordinates:

$$\mathcal{P} = \sum_{i=1}^{n} m_i g^T r_{ci} \tag{4.6}$$

,

where m_i is the mass of the i-th link and r_{ci} it's centre of mass and g is the vector of gravity in the inertial frame. It is important to note that if there is any elasticity in the joints of the robots then one must account for this in the potential energy. The Lagrangian equation is then defined by:

$$\frac{d}{dt}\left(\frac{\partial \mathcal{L}(q,\dot{q})}{\partial \dot{q}_k}\right) - \frac{\partial \mathcal{L}(q,\dot{q}}{\partial q_k} = \tau_k \quad k = 1,\ldots,n \tag{4.7}$$

This equation can be rewritten as:

$$D(q)\ddot{q} + C(q,\dot{q})\dot{q} + G(q) = \tau \tag{4.8}$$

Where in the Coriolis matrix C each element is defined by:

$$c_{kj} = \sum_{i=1}^{n} \frac{1}{2}\left[\frac{\partial d_{kj}}{\partial q_j} + \frac{\partial d_{ki}}{\partial q_j} - \frac{\partial d_{ij}}{\partial q_k}\right] \tag{4.9}$$

and the gravity vector $G(q) = [g_1(q), \ldots g_n(q)]^T$ and τ_k is the generalized force at joint k. When we consider the actuator dynamics (4.8) becomes:

$$M(q)\ddot{q} + C(q,\dot{q})\dot{q} + G(q) = B(q)u \tag{4.10}$$

Where $M(q) = D(q) + J(q)$ here $J(q)$ represent the different inertias present in the actuators and is diagonal, B(q) is an $n \times m$ matrix of full rank, $u \in \mathbb{R}^m$ is the required actuator torque and the control input to the system.

Since the matrix M has the same properties as D(positive definite) it is invertible and one can express the acceleration $\ddot{q}$, by:

$$\ddot{q} = M(q)^{-1}\left[B(q)u - C(q,\dot{q})\dot{q} - G(q)\right] \tag{4.11}$$

To write the system on standard form given by:

$$\dot{x} = f(x) + g(x)u \tag{4.12}$$

we define $x_1 := q$ and $x_2 := \dot{q}$ and thus $x = [x_1, x_2]^T$ this leads to:

$$\begin{aligned} \dot{x_1} &= x_2 \\ \dot{x_2} &= M(x_1)^{-1}\left[B(x_1)u - C(x_1,x_2)x_2 - G(x_1)\right] \end{aligned} \tag{4.13}$$

By inspection:

$$\begin{aligned} f(x) &= \begin{bmatrix} x_2 \\ M(x_1)^{-1}\left(-C(x_1,x_2)x_2 - G(x_1)\right) \end{bmatrix} \\ &\text{and,} \\ g(x) &= \begin{bmatrix} 0 \\ M(x_1)^{-1}B(x_1) \end{bmatrix} \end{aligned} \tag{4.14}$$

4.4 Fully Actuated and Underactuated systems

Underactuated mechanical systems are systems where the number of actuators are fewer than the degrees of freedom. A system on the form of (4.10) is fully actuated when $rank(B(q)) = m = n$, otherwise it is underactuated by degree $n - m$. If the system is fully actuated($rank(B(q)) = n$) then it is invertible and the input u can be expressed as:

$$u = B(q)^{-1} \left[M(q)a_q + C(q, \dot{q})\dot{q} + G(q) \right] \tag{4.15}$$

This type of control action is called inverse dynamics control [54, p. 295]. Inserting this into (4.11) we have:

$$\begin{aligned} \ddot{q} &= M(q)^{-1} \left(B(q)B(q)^{-1} \left[M(q)a_q + C(q, \dot{q})\dot{q} + G(q) \right] - C(q, \dot{q})\dot{q} - G(q) \right) \\ &= M(q)^{-1} \left(M(q)a_q + C(q, \dot{q})\dot{q} + G(q) - C(q, \dot{q})\dot{q} - G(q) \right) \\ &= a_q \end{aligned} \tag{4.16}$$

Where $a_q = \ddot{q}$ is the input acceleration vector. The system in (4.13) now reduces to a double integrator:

$$\begin{aligned} \ddot{x_1} &= x_2 \\ \ddot{x_2} &= a_q \end{aligned} \tag{4.17}$$

The whole system can now be viewed as an inner-loop/outer-loop architecture illustrated in 4.2 where the inner loop calculates the in*f*put u to the robot based on joint positions and velocities, and the outer loop output a_q. A simple choice for the outer loop is for instance:

$$a_q = \ddot{q}_d(t) - K_1 e(t) - K_2 \dot{e}(t) \tag{4.18}$$

Where q_d is the desired trajectory, $e = q - q_d$, $\dot{e} = \frac{d}{dt}e$. K_1 and K_2 are diagonal gain matrices.

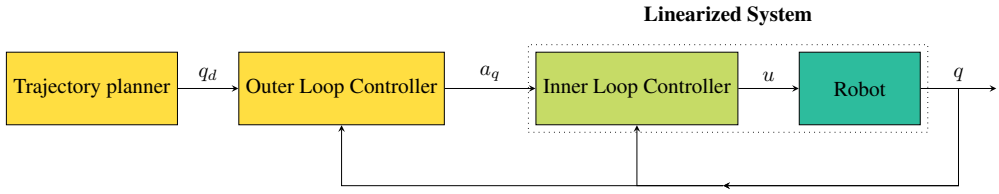

Figure 4.2: Inner-loop/outer-loop structure

The inner loop is now a linearized system. Which is easily controlled.

If the system in (4.10) is underactuated however($rank(B(q) = m < n$) there exists no such direct feedback linerization as in (4.15). To linearize underactuated systems one can use the methoth of partial feedback linearization [53] [1].

[1] Other control objectives will be further discussed later in the text

4.5 Periodic systems and their properties

Many natural systems are periodic examples include planetary motions, bipedal walking and most relevant for this project rising and sitting motions one might also want to induce periodic solutions of other systems. A system has a periodic solution $x(t)$ with period $T > 0$ if[2]:

$$x(t) = x(t+T), \quad \forall t \leq 0, \tag{4.19}$$

A periodic solution on the phase portrait is a closed trajectory and may be referred to as alternatively a *periodic orbit* or a *closed orbit*[21, p. 54-55].

4.5.1 Existence

When we consider second order autonomous/time-invariant[3] systems:

$$\dot{x} = f(x), \quad x \in \mathbb{R}^n \tag{4.20}$$

$f(x)$ is a continuously differentiable function. A condition for (4.20) having a periodic solution is the Poincaré-Bendixson Criterion.

Lemma 4.5.1 (Poincaré-Bendixson Criterion[21])**.** *Consider the system* (4.20) *and let* M *be a closed bounded subset of the plane such that*

- M *contains no equilibrium points, or contains only one equilibrium points such that the Jacobian matrix* $\frac{\partial f}{\partial x}$ *at this point has eigenvalues with positive real parts. (Hence, the equilibrium point is unstable focus or unstable node.)*
- *Every trajectory starting in* M *stays in* M *for all future time.*

Then, M *contains a periodic orbit of* (4.20)*.*

To illustrate the use of the Criterion(lemma 4.5.1) suppose that the equilibrium point P of figure 4.3 has the required properties then all trajectories in the vicinity of it will be moving away from the equilibrium point. We can then choose the closed bounded region M as the shaded area R. If we consider a simple closed curve $V(x) = c$ where $V(x) \in C^1$. Where C^1 is the class of functions that are differentiable and whose derivatives are continuous. The vector field $f(x)$ points inward at x on the curve $V(x)$ if the inner product of the field and the gradient of the curve is negative:

$$f(x) \cdot \nabla V(x) < 0. \tag{4.21}$$

conversely the vector field points outward if:

$$f(x) \cdot \nabla V(x) > 0. \tag{4.22}$$

[2]Trivial solutions $x(t) = c \quad \forall t > 0$ fit the definition (4.19) these solutions correspond to equilibrium points and will be referred to as trivial periodic solutions, otherwise it can be assumed that periodic solutions refer to nontrivial ones.

[3]Meaning no explicit dependence on time, t. In contrast to $\dot{x} = f(x, t)$

Trajectories can only leave the set $M = R$ if the vector field points out of the set at the boundaries. So if $f(x) \cdot \nabla v(x) < 0$ in the shaded area and $f(x) \cdot \nabla V(x) > 0$ in the non-shaded area between P and R, then trajectories stay inside of R. Thus the there must be at least one periodic trajectory C in R. If this periodic trajectory is isolated it is called a *Limit Cycle*.

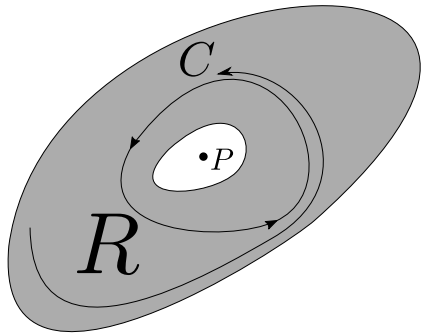

Figure 4.3: Illustration of Poincaré - Bendixson Criterion.Reprinted under Creative Commons License[55]

4.5.2 Orbital stability

The definitions of *Orbital stability* in this text is based on [48], [50] and [21, p 331].

Definition 4.5.1 (Orbital Stability)**.** Let $x^*(t)$ be the solution of (4.20) such that $x^* = x^*(t, x_0^*)$ and $x^*(t) = x^*(t+T), \forall t, T > 0$ meaning that $x^*(t)$ is a periodic solution. Let $\mathcal{O}_{x^*} \subset \mathbb{R}^n$ be the orbit of $x^*(t)$ meaning:

$$\mathcal{O}_{x^*} = \{\zeta \in \mathbb{R}^n : \zeta = x^*(t), t \in [0, T]\} \tag{4.23}$$

and the minimum distance from x to a point in the set M is defined as:

$$dist(x, M) \inf_{y \in M} \|x - y\| \tag{4.24}$$

Then $x^*(t)$ is orbitally stable if for any $\epsilon > 0 \quad \exists \delta > 0$ such that:

$$\text{if} \quad \|x(0) - x_0^*\| < \delta, \quad \text{then} \quad dist(x(t), \mathcal{O}_{x^*}) < \epsilon \quad \forall t \geq 0 \tag{4.25}$$

if this holds and additionally:

$$\lim_{t \to +\infty} dist(x(t), \mathcal{O}_{x^*}) = 0 \tag{4.26}$$

Then it is asymptotically orbitally stable

finally it is orbitally exponentially stable if it is orbitally stable and there exist $c_1, c_2 > 0$ and one can chose $\delta > 0$ such that:

$$\text{if} \quad dist(x_0, \mathcal{O}_{x^*}) < \delta \quad \text{then} \quad dist(x(t), \mathcal{O}_{x^*}) \leq c_1 \cdot dist(x_0, \mathcal{O}_{x^*}) e^{-c_2(t - t_o)}, \forall t \geq t_0 \tag{4.27}$$

4.5.3 Moving Poincaré sections

If one considers the matrix form of (4.7):

$$\frac{d}{dt}\left(\frac{\partial \mathcal{L}(q,\dot{q})}{\partial \dot{q}}\right) - \frac{\partial \mathcal{L}(q,\dot{q}}{\partial q}) = B(q)u \tag{4.28}$$

where $q, \dot{q} \in \mathbb{R}^n$ are the generalized coordinates and their velocities. $u \in \mathbb{R}^m$ are the control inputs and $B(q)$ has full rank. To determine stability of periodic orbits we can introduce *moving Poincaré sections*

Definition 4.5.2 (Moving Poincaré sections[50][24][49])**.** Let $q^*(t)\ \forall\ t\ \in\ [0,T]$ be a solution of (4.28) with the control input $u^*(t)\ \in\ C^1([0,T])$, and initial conditions $q^*(0) = q_0^*, \dot{q}^*(0) = \dot{q}_0^*$, such that $(|\dot{q}^*(t)|^2 + \ddot{q}^*(t)) > 0\ \forall t \in [0,T]$. The corresponding trajectory´s orbit:

$$\mathcal{O}_{q^*} = \left\{ \left[\begin{smallmatrix} q \\ \dot{q} \end{smallmatrix} \right] \in \mathbb{R}^{2n} : q = q^*(\tau), \dot{q} = \dot{q}^*(\tau), \tau \in [0,T] \right\}, \tag{4.29}$$

and the tubular neighborhood, the set of all points no further than some $\epsilon > 0$ from $\mathcal{O}^*$:

$$\mathcal{O}_\epsilon(q^*) = \left[\begin{smallmatrix} q \\ \dot{q} \end{smallmatrix} \right] : \min_{\tau \in [0,T]} \|[q - q^*(\tau); \dot{q} - \dot{q}^*(\tau)]\| \leq \epsilon \tag{4.30}$$

A *Moving Poincaré Section* is a family if $(2n-1)$-dimensional C^1-smooth surfaces $S(t), t \in [0,T]$ associated with $q^*(t)$, if:

1. Surfaces $S(\cdot)$ are locally disjoint meaning $\exists \epsilon > 0 : S(\tau_1) \cap S(\tau_2) \cap \mathcal{O}_\epsilon^* = \emptyset, \forall \tau_1, \tau_2, \tau_1 \neq \tau_2$.

2. Each of the surfaces $S(\cdot)$ locally intersects the orbit only at one point, meaning $\exists \epsilon > 0 : S(\tau) \cap \left\{ \left[\begin{smallmatrix} q^*(t) \\ \dot{q}^*(t) \end{smallmatrix} \right], |t - \tau| < \epsilon \right\} \cap \mathcal{O}_\epsilon(q^*) = \left\{ \left[\begin{smallmatrix} q^*(\tau) \\ \dot{q}^*(\tau) \end{smallmatrix} \right] \right\} \forall \tau \in [0,T]$.

3. The surfaces $S(\cdot)$. are smoothly parametrized by time, meaning $\exists f_s(q,\dot{q},t)\ \in\ C^1(\mathbb{R}^n, \mathbb{R}^n, \mathbb{R})$ and $\epsilon > 0 : S(t) \cap \mathcal{O}_\epsilon(q^*) = \{ \left[\begin{smallmatrix} q \\ \dot{q} \end{smallmatrix} \right] \in \mathbb{R}^{2n} : f_s(q,\dot{q},t) = 0 \} \cap \mathcal{O}_\epsilon(q^*)$.

4. The surfaces $S(\cdot)$ are transversal to the orbit (4.29), meaning $\forall t \in [0,T]$:

$$\left[\left. \frac{\partial f_s}{\partial q} \right|_{\substack{q=q^*(t) \\ \dot{q}=\dot{q}^*(t)}} \right]^T \dot{q}^*(t) + \left[\left. \frac{\partial f_s}{\partial \ddot{q}} \right|_{\substack{q=q^*(t) \\ \dot{q}=\dot{q}^*(t)}} \right]^T \ddot{q}^*(t) \neq 0.$$

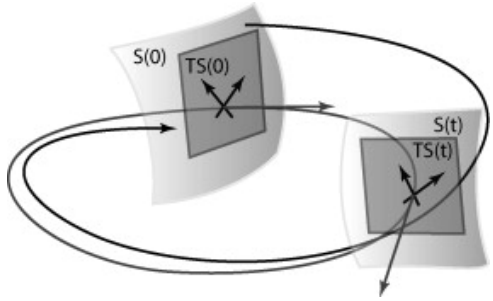

Figure 4.4: Moving Poincaré section for periodic trajectory $x^*(t)$. Reprinted from Annual Reviews in Control Vol.32, Issue 2, A.S. Shiriaev, L.B. Freidovich, I.R. Manchester , Can we make a robot ballerina perform a pirouette? Orbital stabilization of periodic motions of underactuated mechanical systems, Pages 200-211, Copyright ©(2008), with permission from Elsevier

4.5.4 Transverse Coordinates

Definition 4.5.3 (Transverse coordinates[49])**.** Given a moving Poincaré section as in definition 4.5.2, the state coordinates can be locally transformed into $\begin{bmatrix} q \\ \dot{q} \end{bmatrix} \mapsto \begin{bmatrix} \theta \\ x_\perp \end{bmatrix}$. $\theta(t) \in \mathbb{R}^1$ parameterizes position on the trajectory in $\mathbb{R}^n \times \mathbb{R}^n$. $x_\perp(t) \in \mathbb{R}^{2n-1}$ defines location on the surface $S(t)$. $x_\perp$ is known as the vector of *transverse coordinates* and belongs to the tangent space $TS(t)$[50] of the moving Poincaré sections as shown in figure 4.4. The dynamics of $x_\perp$ is known as the *transverse dynamics*.

If one linearizes the transverse dynamics as in definition 4.5.3 along the solution $q^*(t), t \in [0, T]$ this brings about a linear time-varying control system defined for $t \in [0, T]$ and is of dimension $2n$. The subsystem $x_\perp$ as defined in 4.5.3 are called a *transverse linearization*, discussed further in 4.6.4.

4.6 Virtual Holonomic constraints (VHC)

Definition 4.6.1 (Virtual holonomic constraints)**.** Given a controlled Lagrangian system like (4.28), suppose there exist a solution q^* and a control input u^* (and not physical constraints) that imposes the following geometric relations:

$$q_1 = \phi_1(\theta), \quad q_2 = \phi_2(\theta), \quad \dots \quad , q_n = \phi_n(\theta) \tag{4.31}$$

between the generalized coordinates and a new variable $\theta \in \mathbb{R}$. The functions $\phi_i(\theta)$ are smooth(C^2) functions. Then the relations (4.31) are called *virtual holonomic constraints*.

The scalar variable θ is alternatively know as the motion generator(MG) and ϕ_i as the synchronization functions. There are many choices for θ, but most often one will choose the coordinate at the passive joint when dealing with underactuated systems.

The idea of *Virtual holonomic constraints approach* is to find some relation between the degrees of freedom or a desired relation and then impose that relation on the system with control action.

4.6.1 Reduced dynamics

Assume that the conditions of 4.6.1 are valid on the orbit of the solution q^*, see (4.29). If the control input u^* achieves holding the relations (4.31) invariant we can rewrite (4.10) by utilising:

$$q(t) = \Phi(\theta^*(t)), \quad \dot{q}(t) = \Phi'(\theta^*)\dot{\theta}^*(t) \quad \text{and} \quad \ddot{q}(t) = \Phi'(\theta^*(t))\ddot{\theta}^*(t) + \Phi''(\theta^*(t))\dot{\theta}^*(t)^2$$

Where

$$\begin{aligned} q(t) &= [q_1(t), q_2(t), \ldots, q_n(t)]^T \\ \dot{q}(t) = \frac{d}{dt}q(t) &= [\dot{q}_1(t), \dot{q}_2(t), \ldots, \dot{q}_n(t)]^T \\ \ddot{q}(t) = \frac{d^2}{dt^2}q(t) &= [\ddot{q}_1(t), \ddot{q}_2(t), \ldots, \ddot{q}_n(t)]^T \end{aligned} \tag{4.32}$$

, and

$$\begin{aligned} \Phi(\theta) &:= [\phi_1(\theta), \phi_2(\theta), \ldots, \phi_n(\theta]^T \\ \Phi'(\theta) = \frac{\partial}{\partial\theta}\Phi(\theta) &= [\phi_1'(\theta), \phi_2'(\theta), \ldots, \phi_n'(\theta]^T \\ \Phi''(\theta) = \frac{\partial^2}{\partial\theta^2}[\phi_1(\theta), \phi_2(\theta), \ldots, \phi_n(\theta]^T &= [\phi_1''(\theta), \phi_2''(\theta), \ldots, \phi_n''(\theta]^T \end{aligned} \tag{4.33}$$

This leads to:

$$\begin{aligned} M(\Phi(\theta^*))\left[\Phi'(\theta^*)\ddot{\theta}^* + \Phi''(\theta^*)\dot{\theta^*}^2\right] + C(\Phi(\theta^*), \Phi'(\theta^*))\dot{\theta}^* \cdot \Phi'(\theta^*)\dot{\theta}^* \\ + G(\Phi(\theta^*)) = B(\Phi(\theta^*))u^* \end{aligned} \tag{4.34}$$

This can be manipulated by introducing

$$B(q)^\perp \in \mathbb{R}^{(n-m)\times n} \quad \text{such that} \quad B(q)^\perp B(q) = 0 \tag{4.35}$$

a matrix that defines the nonactuated coordinates such that[32]:

$$\begin{aligned} B^\perp(\Phi(\theta^*))\Bigg[M(\Phi(\theta^*))\left[\Phi'(\theta^*)\ddot{\theta}^* + \Phi''(\theta^*)\dot{\theta^*}^2\right] \\ + C(\Phi(\theta^*), \Phi'(\theta^*))\dot{\theta}^* \cdot \Phi'(\theta^*)\dot{\theta}^* + G(\Phi(\theta^*))\Bigg] \\ = B^\perp(\Phi(\theta^*))B(\Phi(\theta^*))u^* = 0 \end{aligned} \tag{4.36}$$

One can then rearrange (4.36) into a set of second order differential equations [52]:

$$\alpha_i(\theta^*)\ddot{\theta}^* + \beta_i(\theta^*)\dot{\theta^*}^2 + \gamma_i(\theta^*) = 0 \quad i = 1, \ldots, n-m. \tag{4.37}$$

(4.37) is known as the *reduced dynamics* Where $\alpha(\cdot), \beta(\cdot)$ and $\gamma(\cdot)$ are smooth functions defined as:

$$\begin{aligned} \alpha(\theta^*) &= B^\perp(\Phi(\theta^*))M(\Phi(\theta^*))\Phi'(\theta^*), \\ \beta(\theta^*) &= B^\perp(\Phi(\theta^*))\left[C(\Phi(\theta^*), \Phi'(\theta^*))\Phi'(\theta^*) + M(\Phi(\theta^*))\Phi''(\theta^*)\right], \\ \gamma(\theta^*) &= B^\perp(\Phi(\theta^*))G(\Phi(\theta^*)). \end{aligned} \tag{4.38}$$

When the degree of underactuation is one this reduces to a scalar second order differential equation:

$$\alpha(\theta^*)\ddot{\theta}^* + \beta(\theta^*)\dot{\theta^*}^2 + \gamma(\theta^*) = 0 \tag{4.39}$$

The whole motion will now be parameterized by the variable θ^*. Meaning that we now can study the full system (4.10) by solving (4.37) and keeping the relations of (4.31) in mind. [32]

Theorem 4.6.1 (Integral of motion of reduced dynamics [51],[50],[32])**.** *Suppose that $\alpha(\theta) \neq 0$ along the solution $(\theta^*(t), \dot{\theta}^*(t))$ with initial conditions $\theta^*(0) = \theta_0, \dot{\theta}^*(0) = \dot{\theta}_0$. Then there exist a integral function I along the solution. The integral of motion of the reduced dynamics* (4.39) *is:*

$$I(\theta^*(t), \dot{\theta}^*(t), \theta_0, \dot{\theta}_0) = \dot{\theta^*}^2 - \psi(\theta^*, \theta_0)\left[\dot{\theta}_0^2 - \int_{\theta_0}^{\theta^*} \psi(s, \theta_0)\frac{2\gamma(s)}{\alpha(s)}ds\right] \tag{4.40}$$

with

$$\psi(\theta_0, \theta_1) = e^{-2\int_{\theta_0}^{\theta_1} \frac{\beta(\tau)}{\alpha(\tau)}d\tau} \tag{4.41}$$

This integral function preserves its zero value along $(\theta^*, \dot{\theta}^*)$ even if $(\theta^*, \dot{\theta}^*)$ are unbounded.

Proof. See B.2 □

Theorem 4.6.2 ([51])**.** *With some constants x and y, the time derivative of the function $I(\theta, \dot{\theta}, x, y)$ as defined in 4.6.1 calculated along the solution $(\theta(t), \dot{\theta}(t))$ of the system:*

$$\alpha(\theta)\ddot{\theta} + \beta(\theta)\dot{\theta}^2 + \gamma(\theta) = W \tag{4.42}$$

can be found as

$$\frac{d}{dt}I(\theta, \dot{\theta}, x, y) = \dot{\theta}\left\{\frac{2}{\alpha(\theta)}W - \frac{2\beta(\theta)}{\alpha(\theta)}I(\theta, \dot{\theta}, x, y)\right\} \tag{4.43}$$

Proof. See B.3 □

4.6.2 Periodic Solution

The goal is to find a feedback controller that achieves invariance of the VHC(4.31) and Orbital Asymptotic stability of a T-periodic solution of (4.37)

$$\theta^*(t) = \theta^*(t + T) \quad \forall t \tag{4.44}$$

4.6.3 Partial Feedback Linearization

Given the virtual holonomic constraints (4.31), we can introduce $(n + 1)$ excessive coordinates

$$y_1 = q_1 - \phi_1(\theta), \quad \ldots, \quad y_n = q_n - \phi_n(\theta) \tag{4.45}$$

for the original system(n-DoF). Since they are excessive we can choose one of the coordinates and express it as a function of the others and thus exclude it. So we are left with

$$y = \begin{bmatrix} y_1 \\ \vdots \\ y_{n-1} \end{bmatrix} \text{ and } \theta. \tag{4.46}$$

The last(arbitrarily chosen) equality in (4.45) can be expressed as

$$q_n = \phi_n(\theta) + h(y_1, \ldots, y_{n-1}, \theta) \tag{4.47}$$

Where $h(\cdot)$ is a smooth(C^2) scalar function and $h(\cdot) \equiv 0$ on $q^*(t)$

$$\begin{aligned} \dot{q} = \begin{bmatrix} \dot{q}_1 \\ \vdots \\ \dot{q}_n \end{bmatrix} &= \begin{bmatrix} \dot{y}_1 + \phi_1'(\theta)\dot{\theta} \\ \dot{y}_2 + \phi_2'(\theta)\dot{\theta} \\ \vdots \\ \phi_n'(\theta)\dot{\theta} + \nabla h \cdot \begin{bmatrix} \dot{y} \\ \dot{\theta} \end{bmatrix} \end{bmatrix} \\ &= \left(\begin{bmatrix} \boldsymbol{I}_{n-1} & \mathbf{0}_{(n-1)\times 1} \\ & \nabla h \end{bmatrix} + \begin{bmatrix} \mathbf{0}_{n\times(n-1)} & \Phi'(\theta) \end{bmatrix} \right) \begin{bmatrix} \dot{y} \\ \dot{\theta} \end{bmatrix} \\ &= L(y,\theta) \begin{bmatrix} \dot{y} \\ \dot{\theta} \end{bmatrix} \end{aligned} \tag{4.48}$$

where $\boldsymbol{I}_{n-1}$ is the $(n-1) \times (n-1)$-identity matrix, $\mathbf{0}_{a\times b}$ is the $a \times b$-zero matrix, $\nabla h = \left[\frac{\partial h}{\partial y_1}, \ldots, \frac{\partial h}{\partial y_{n-1}}, \frac{\partial h}{\partial \theta} \right]$, and $\Phi'(\theta)$ as in (4.33).

$$\begin{aligned} \ddot{q} = \begin{bmatrix} \ddot{q}_1 \\ \vdots \\ \ddot{q}_n \end{bmatrix} &= \begin{bmatrix} \ddot{y}_1 + \phi_1''(\theta)\dot{\theta}^2 + \phi_1'(\theta)\ddot{\theta} \\ \ddot{y}_2 + \phi_2''(\theta)\dot{\theta}^2 + \phi_1'(\theta)\ddot{\theta} \\ \vdots \\ \phi_n''(\theta)\dot{\theta}^2 + \phi_n'(\theta)\ddot{\theta} + \frac{d}{dt}\left(\nabla h \cdot \begin{bmatrix} \dot{y} \\ \dot{\theta} \end{bmatrix} \right) \end{bmatrix} \\ &= L(y,\theta) \begin{bmatrix} \ddot{y} \\ \ddot{\theta} \end{bmatrix} + \begin{bmatrix} \mathbf{0}_{(n-1)\times 1} \\ 1 \end{bmatrix} \begin{bmatrix} \dot{y}^T & \dot{\theta} \end{bmatrix} \nabla^2 h \begin{bmatrix} \dot{y} \\ \dot{\theta} \end{bmatrix} + \Phi''(\theta)\dot{\theta}^2 \\ &= L(y,\theta) \begin{bmatrix} \ddot{y} \\ \ddot{\theta} \end{bmatrix} + N(y,\theta,\dot{y},\dot{\theta}) \end{aligned} \tag{4.49}$$

Where $\nabla^2 h$ is the Hessian of the function $h(y_1, y_2, \ldots, y_{n-1}, \theta)$. This transformation can now be used to rewrite the (4.11) in terms of the new coordinates

$$L(y,\theta) \begin{bmatrix} \ddot{y} \\ \ddot{\theta} \end{bmatrix} + N(y,\theta,\dot{y},\dot{\theta}) = M(y,\theta)^{-1} \left[B(y,\theta)u - C(\theta,\dot{\theta},y,\dot{y}) L(y,\theta) \begin{bmatrix} \dot{y} \\ \dot{\theta} \end{bmatrix} - G(y,\theta) \right] \tag{4.50}$$

Suppose that $L(y,\theta)$ is nonsingular in a vicinity of the orbit $\mathcal{O}_{\theta^*}$ of a solution $\theta^*(t)$ then we can rewrite (4.50) as

$$\begin{bmatrix}\ddot{y}\\ \ddot{\theta}\end{bmatrix} = L(y,\theta)^{-1}\left\{M(y,\theta)^{-1}\left[B(y,\theta)u - C(y,\theta,\dot{y},\dot{\theta})L(y,\theta)\begin{bmatrix}\dot{y}\\ \dot{\theta}\end{bmatrix} - G(y,\theta)\right] - N(y,\theta,\dot{y},\dot{\theta})\right\} \tag{4.51}$$

Looking at the $(n-1)$ subsystem $\ddot{y}$

$$\ddot{y} = K(y,\theta)u + R(y,\theta,\dot{y},\dot{\theta}) \tag{4.52}$$

where

$$K(y,\theta) := \begin{bmatrix}I_{n-1}\\ \mathbf{0}_{(n-1)\times 1}\end{bmatrix}^T L(y,\theta)^{-1}M(y,\theta)^{-1}B(y,\theta) \tag{4.53}$$

and

$$\begin{aligned}R(y,\theta,\dot{y},\dot{\theta}) = \begin{bmatrix}I_{n-1}\\ \mathbf{0}_{(n-1)\times 1}\end{bmatrix}^T L(y,\theta)^{-1}\Bigg\{M(y,\theta)^{-1}\Bigg[- C(y,\theta,\dot{y},\dot{\theta})L(y,\theta)\begin{bmatrix}\dot{y}\\ \dot{\theta}\end{bmatrix}\\ - G(y,\theta)\Bigg] - N(y,\theta,\dot{y},\dot{\theta})\Bigg\}\end{aligned} \tag{4.54}$$

From here on out we will assume that the degree of underactuation is one$(m = n-1)$**)** If we introduce a feedback transformation on the form:

$$u = K(y,\theta)^{-1}[v - R(y,\theta,\dot{y},\dot{\theta})] \tag{4.55}$$

then (4.52) is reduced to

$$\begin{aligned}\ddot{y} =& K(y,\theta)\left\{K(y,\theta)^{-1}[v - R(y,\theta,\dot{y},\dot{\theta})]\right\} + R(y,\theta,\dot{y},\dot{\theta})\\ =& v\end{aligned} \tag{4.56}$$

Where $v \in \mathbb{R}^(n-1)$ is a new control input that will be discussed later. When it comes to the dynamics of θ we use $B^\perp \in \mathbb{R}^{1\times n}$ as defined in (4.35) and multiply it by (4.50)

$$\begin{aligned}&B^\perp(y,\theta)\left\{M(y,\theta)\left[L(y,\theta)\begin{bmatrix}\ddot{y}\\ \ddot{\theta}\end{bmatrix} + N(y,\theta,\dot{y},\dot{\theta})\right]\right\}\\ &= B^\perp(y,\theta)\left\{\left[B(y,\theta)u - C(\theta,\dot{\theta},y,\dot{y})L(y,\theta)\begin{bmatrix}\dot{y}\\ \dot{\theta}\end{bmatrix} - G(y,\theta)\right]\right\}\\ &\Rightarrow B^\perp(y,\theta)\left\{M(y,\theta)\left[L(y,\theta)\begin{bmatrix}\ddot{y}\\ \ddot{\theta}\end{bmatrix} + N(y,\theta,\dot{y},\dot{\theta})\right] + C(\theta,\dot{\theta},y,\dot{y})L(y,\theta)\begin{bmatrix}\dot{y}\\ \dot{\theta}\end{bmatrix} + G(y,\theta)\right\}\\ &= B^\perp(y,\theta)B(y,\theta)u = 0\end{aligned} \tag{4.57}$$

and use *Hadamard's lemma*(A.2.1) when $y = \dot{y} = \ddot{y} = \mathbf{0}_{(n-1)\times 1}$ and eliminate $\ddot{y}$ by using (4.56) we rediscover the $\alpha - \beta - \gamma$-equation of the reduced dynamics:

$$\begin{aligned} \alpha(\theta)\ddot{\theta} + \beta(\theta)\dot{\theta}^2 + \gamma(\theta) &= g_y(y,\theta,\dot{y},\dot{\theta},\ddot{\theta})y + g_{\dot{y}}(y,\theta,\dot{y},\dot{\theta},\ddot{\theta})\dot{y} \\ &\quad + g_v(y,\theta,\dot{y},\dot{\theta},\ddot{\theta})v \\ \ddot{y} &= v \end{aligned} \tag{4.58}$$

$g_y(\cdot), g_{\dot{y}}(\cdot), g_v(\cdot)$, are all smooth functions of the requisite dimensions.

4.6.4 Transverse linearization

A natural choice of transverse coordinates are

$$x_\perp = \begin{bmatrix} I(\theta,\dot{\theta},\theta_0^*,\dot{\theta}_0^*) \\ y \\ \dot{y} \end{bmatrix} \in \mathbb{R}^{2n-1} \tag{4.59}$$

Where I is as defined in 4.6.1. These transverse coordinates represent a deviation from the orbit of θ^* because if a at any point in the vicinity $x_\perp = 0$ then that point belongs to $\mathcal{O}_{\theta^*}$ and if not then magnitude of $x_\perp$ is equal to the Euclidean distance to the orbit from that point [38].

4.6.5 Augmented system

Based on:[51] By using Theorem 4.6.2 we can introduce

$$\begin{aligned} \frac{d}{dt}I(\theta,\dot{\theta},\theta_0^*,\dot{\theta}_0^*) &= \frac{2\dot{\theta}}{\alpha(\theta)}\left\{[\tilde{g}_y(\cdot)y + \tilde{g}_{\dot{y}}(\cdot)\dot{y} + \tilde{g}_v(\cdot)v] - \beta(\theta)I(\theta,\dot{\theta},\theta_0^*,\dot{\theta}_0^*)\right\} \\ \ddot{y} &= v \end{aligned} \tag{4.60}$$

where

$$\begin{aligned} \tilde{g}_y &= g_y(0,\theta^*(t),0,\dot{\theta}^*(t),\ddot{\theta}^*(t)) \\ \tilde{g}_{\dot{y}} &= g_{\dot{y}}(0,\theta^*(t),0,\dot{\theta}^*(t),\ddot{\theta}^*(t)) \\ \tilde{g}_v &= g_v(0,\theta^*(t),0,\dot{\theta}^*(t),\ddot{\theta}^*(t)) \end{aligned} \tag{4.61}$$

The linear control system of (4.60) along with the definition of $x_\perp$ as in (4.59) gives us on state-space form:

$$\dot{x}_\perp = A(t)x_\perp + b(t)v \tag{4.62}$$

Where $A(t) \in \mathbb{R}^{(2n-1)\times(2n-1)}$ and $b(t) \in \mathbb{R}^{(2n-1)\times(n-1)}$ are defined as:

$$A(t+T) = A(t) = \begin{bmatrix} a_{11}(t) & a_{12}(t) & a_{13}(t) \\ \mathbf{0}_{(n-1)\times 1} & \mathbf{0}_{(n-1)\times(n-1)} & I_{n-1} \\ \mathbf{0}_{(n-1)\times 1} & \mathbf{0}_{(n-1)\times(n-1)} & \mathbf{0}_{(n-1)\times(n-1)} \end{bmatrix} \tag{4.63}$$

$$b(t+T) = b(t) = \begin{bmatrix} b_1(t) \\ \mathbf{0}_{(n-1)\times(n-1)} \\ I_{n-1} \end{bmatrix}$$

Where

$$\begin{aligned} a_{11}(t) &= -\frac{2\dot{\theta}^*(t)\beta(\theta^*(t))}{\alpha(\theta^*(t))}, \quad a_{12}(t) = \frac{2\dot{\theta}^*(t)\tilde{g}_y(\cdot)}{\alpha(\theta^*(t))}, \\ a_{13}(t) &= \frac{2\dot{\theta}^*(t)\tilde{g}_{\dot{y}}(\cdot)}{\alpha(\theta^*(t))} \qquad\qquad b_1(t) = \frac{2\dot{\theta}^*(t)\tilde{g}_v(\cdot)}{\alpha(\theta^*(t))} \end{aligned} \tag{4.64}$$

4.7 Stabilizing linear systems

For a general linear system

$$\begin{aligned} \dot{x}(t) &= A(t)x(t) + b(t)u(t) \quad \forall t \in [t_0, T] \\ y(t) &= C(t)x(t) \end{aligned} \tag{4.65}$$

Where the state vector $x(t) \in \mathbb{R}^n$, input vector $u(t) \in \mathbb{R}^m$, $A(t) \in \mathbb{R}^{n\times n}, b(t) \in \mathbb{R}^{n\times m}$ and $C(t) \in \mathbb{R}^{p\times n}$.

Definition 4.7.1 (Exponential Stability[21])**.** The equilibrium point $x = 0$ of (4.65) is exponentially stable if there exits positive constants c, k and λ such that

$$\|x(t)\| \leq k\|x(t_0)\|e^{-\lambda(t-t_0)}, \forall \|x(t_0)\| < c \tag{4.66}$$

and globally exponentially stable if (4.66) for any initial state $x(t_0)$

If $A(t) = A$, meaning constant and the conditions of Definition 4.7.1 holds then A is called a *Hurwitz* matrix and $Re[\lambda_i] < 0 \forall i$ where λ_i, are the eigenvalues of A.

Theorem 4.7.1 (Controllability [7])**.** *The n-dimensional pair $(A(t), b(t)$ is controllable at time t_0 if and only if there exists $t_1 > t_0$ such that*

$$\mathbf{W}_c(t_0, t_1) = \int_{t_0}^{t_1} \mathbf{\Phi}(t_1, \tau)b(\tau)b(\tau)^T\mathbf{\Phi}(t_1, \tau)^T d\tau \tag{4.67}$$

and $\mathbf{W}_c \in R^{n\times n}$ is nonsingular Where $\mathbf{\Phi}(\mathbf{t}, \tau)$ is the state transition matrix of $\dot{x} = A(t)x(t)$ as defined in A.3.2.

Proof. See B.4 □

4.7.1 State Feedback Control

Based on:[57][5] If the controllability conditions of theorem 4.7.1 are met for (4.65) we can introduce the control input

$$u(t) = K(t)x(t) \tag{4.68}$$

$K(t)$ is chosen such that $(A + bK)$ is a stable matrix. This leads to the closed loop system

$$\dot{x} = [A(t) - b(t)K(t)]\, x(t) \tag{4.69}$$

The equilibrium $x(t) = 0$ is exponentially stable. The existence of such a matrix(K) is guaranteed if (A, b) are controllable(or stabilizable)[18]

4.7.2 Linear-quadratic Regulator

To find the optimal control input (4.68) one minimizes a quadratic cost function J

$$J(x(t_0), u(t), t_0, t_1) = \int_{t_0}^{t_1} \left[x(t)^T q(t) x(t) + u(t)^T R(t) u(t)\right] dt + x(t_1)^T S x(t_1) \tag{4.70}$$

$Q(t)$ is the weight of deviation of the state $x(t)$ from the origin, $R(t)$ is the weight on the use of control action and $S(t)$ is the weight on the final state. Where $Q \in \mathbb{R}^{n\times n} = Q^T \succeq 0$(Symmetric positive-semidefinite), $R \in \mathbb{R}^{m\times m} = R^T \succ 0$(Symmetric positive-definite) and $S \in \mathbb{R}^{n\times n} = S^T \succeq 0$.

The optimal control is then

$$u^*(t) = -R(t)^{-1} P(t) x(t) \tag{4.71}$$

Where $P(t) = P^T(t)$ is the solution of the *Riccati differential equation*(RDE)[20].

$$-\dot{P}(t) = A^T(t)P(t) + P(t)A(t) - P(t)B(t)R^{-1}(t)B^T(t)P(t) + Q(t) \quad \text{and} \quad P(t_1) = S \tag{4.72}$$

4.8 Periodic Riccati differential equation

[4]

To stabilize the origin of the augmented system (4.62) corresponding to the nominal behaviour i.e

$$\begin{aligned} &I = 0 \\ &y = 0 \rightarrow q_i = \phi_i(\theta^*) \quad i = 1, \ldots, n-1 \\ &\dot{y} = 0 \rightarrow \dot{q}_i = \phi_i'(\theta^*)\dot{\theta}^* \quad i = 1, \ldots, n-1 \end{aligned} \tag{4.73}$$

one finds the LQR-gain matrix $K(t)$ by solving the matrix Riccatti differential equation with Periodic coefficients(PRDE) (4.75) with (4.74).

$$P(t) = P(t+T) \quad \text{and} \quad P(t) = P(t)^T \quad \text{for all} \quad t \in [0, T] \tag{4.74}$$

and

$$\dot{P}(t) + A(t)^T P(T) + P(t)A(t) + Q(t) = P(t)b(t)R(t)^{-1}b(t)^T P(t) \quad \forall t \in [0, T]. \tag{4.75}$$

Where Q and R are constant weights on the state and control input respectively, $A(t)$ and $B(t)$ are as defined in (4.63). This equation can then be solved numerically as shown in [51]. This leads to the expression for K in (4.76)

$$K(t) = -R^{-1}b(t)^T P(t) \tag{4.76}$$

[4]This section is largely taken from the TTK4550 - Engineering Cybernetics, Specialization Project, which is appended to the text.

This $K(t)$ minimizes the quadratic cost function:

$$J = \int_0^\infty \left[x(t)^T Q(t)x(t) + u(t)^T R(t)u(t)\right]\, dt \tag{4.77}$$

wrt. $u(t)$ on solutions of the periodic system:

$$\dot{x}(t) = A(t)x(t) + b(t)u(t), \quad x(0) = x_0 \tag{4.78}$$

(4.77) and (4.78) as presented in [13]

4.8.1 Preliminaries

Theorem 4.8.1 ([59]). *First consider the state transition matrix as defined in Definition A.3.2. If $A(t)$ is T-periodic then the monodromy matrix corresponding to $A(t)$ is*

$$\Psi_A(t_0) = \Phi_A(t_0 + T, t_0) \tag{4.79}$$

and the eigenvalues of $\Psi_A(t_0)$ are called the characteristic multipliers of $A(t)$[59][13].

Definition 4.8.1 (Reachable). A characteristic multiplier λ of $A(t)$ is said to be *unreachable* if $\Psi_A^T(0)x = \lambda x, x \neq 0$ imply that $b(t)^T\Phi_A^T(0,t) = 0$ almost everywhere for $t \in [0,T]$. Conversely if λ of $A(t)$ is not unreachable than it it is *reachable*.

Definition 4.8.2 (Stabilizable). The system (4.65) is said to be *stabilizable* if all characteristic multipliers $|\lambda| \geq 0$ are reachable

Definition 4.8.3 (Observability). A characteristic multiplier λ of $A(t)$ is said to be *unobservable* if $\Psi_A^T(0)x = \lambda x, x \neq 0$ imply that $C(t)^T\Phi_A^T(0,t) = 0$ almost everywhere for $t \in [0,T]$. Conversely if λ of $A(t)$ is not unobservable than it it is *observable*.

Definition 4.8.4 (Detectability). The system (4.65) is said to be *detectable* if all characteristic multipliers $|\lambda| \geq 0$ are observable

Definition 4.8.5 (Stabilizing solution). A solution $P(t)$ is called a *stabilizing solution* if $A(t) - b(t)b(t)^T P(t)$is stable.

Theorem 4.8.2 (Existence[59]). *The periodic Riccati differential equation* (4.75) *has a unique T-periodic stabilizing solution $P(t) = P(t)^T \succeq 0$ if an only if the pair $(A(t), b(t)$ is stabilizable and the pair $(A(t), C(t))$ is detectable*

Theorem 4.8.3 (Existence [13]). *The periodic Riccati differential equation* (4.75) *has a unique T-periodic stabilizing solution $P(t) = P(t)^T \succeq 0$ if the pair $(A(t), b(t)$ is stabilizable and the pair $(A(t), Q(t)^{\frac{1}{2}}$ is detectable, where $(Q(t)^{\frac{1}{2}})^T Q(t)^{\frac{1}{2}} = Q(t)$*

There are numerous methods for solving the PRDE(4.75)(and it is also an area of active research)like the periodic generator method[66], multishot methods[59], but here we will consider the approaches in [14][15]

4.8.2 Solving the periodic differential Riccati equation

Consider the differential Riccati equation

$$\mathcal{R}(P,t) = 0, \quad \forall t \geq 0, \tag{4.80}$$

Where $\mathcal{R}(P,t)$ is defined as

$$\mathcal{R}(P,t) = \frac{d}{dt}P(t) + A(t)^T P(t) + P(t)A(t) - P(t)Bt)R(t)^{-1}B(t)^T P(t) + Q(t) \tag{4.81}$$

$A(t), Q(t), P(t) \in \mathbb{R}^{n\times n}$, $B(t) \in \mathbb{R}^{n\times m}$, $R(t) \in \mathbb{R}^{m\times m}$ all these matrices are continous and T-periodic matrix-functions with $T > 0$, $Q(t), R(t) \succ 0 \quad \forall t \geq 0$.

Proposition 4.8.1 (Maximal solution of (4.81)[14][15])**.** *Suppose that A, B, Q, and R are continuous T-periodic matrix-functions, the pair (A, B) is stabilizable and $Q(t) \succ 0$, $R(t) \succ 0$, $\forall\, t \in [0, T]$. Then, there exists a T-periodic stabilising solution P^+ of* (4.81)*. Moreover, any T-periodic solution P of the Riccati inequality*

$$\mathcal{R}(P,t) \geq 0 \quad \forall t \in [0,T], \tag{4.82}$$

satisfies the inequality

$$P(t) \leq P^+(t) \quad \forall t \in [0,T]. \tag{4.83}$$

The Schur complement[5]transforms (4.82) into a linear matrix inequality(LMI) [14]

$$\mathcal{L}(P,t) \geq 0, \quad \forall t \in [0,T], \tag{4.84}$$

where

$$\mathcal{L}(P,t) = \begin{bmatrix} \frac{d}{dt}P(t) + A(t)^T P(t) + P(t)A(t) + Q(t) & P(t)B(t) \\ B(t)^T P(t) & R(t) \end{bmatrix} \tag{4.85}$$

(4.83) means that the problem of finding this periodic matrix function now is a optimisation problem by using the performance index

$$\mathcal{F}(P) = \int_0^T tr(P(t))dt \tag{4.86}$$

where $tr(A(t)) = \sum_{i=1}^{n} a_{ii}(t)$ for any $A(t) \in \mathbb{R}^{n\times n}$. (4.86). Minimizing the performance index with the inequality (4.85) is an infinite dimensional problem. To find an finite approximation of a stabilizing solution one introduces a T-periodic trigonometric symmetric matrix polynomial $\hat{P} \in \mathbb{R}^{n\times n}$

$$\hat{P} = \sum_{k=-M}^{M} e^{\mathbf{i}k\omega t} F_k(P) \tag{4.87}$$

[5]Schur complement of M[42] :$(M/P) = S - RP^{-1}Q$, where the nonsingular P is the leading submatrix of $M = \begin{bmatrix} P & Q \\ R & S \end{bmatrix}$

Where **i** is the imaginary unit, $\omega = \frac{2\pi}{T}$, $F_0(P)^T = F_0(P) \in \mathbb{R}^{n\times n}$, $F_k(P)^T = F_k(P) \in \mathbb{C}^{n\times n}$ Let $\mathcal{P}_M$ be the vector space of all matrix polynomials $\hat{P}$ of degree $\leq M$.

To transform infinite optimization problem into a finite one we consider a sampled version of (4.85)

$$\mathcal{L}(P, t_j) \geq 0, \quad t_j = (j-1)\frac{T}{N}, \quad j = 1, \ldots, N \tag{4.88}$$

Thus, we have the Semi-definite programming(SDP) problem:

$$\begin{aligned} &\min_{\hat{P}(t_j)\in\mathcal{P}_M} \quad -\mathcal{F}(\hat{P}) \\ &\text{s.t.} \\ &\mathcal{L}(\hat{P}, t_j) \geq 0 \quad j = 1, \ldots, N \\ &-dI_n \leq \hat{P}(t_j) \leq dI_n \quad j = 1, \ldots, N \end{aligned} \tag{4.89}$$

Where d is a constant, chosen sufficiently large, I_n is the $n \times n$ identity matrix

5

Experiment

5.1 Hypothesis

Hypothesis 1 (H1)**.** *There exists functions $\phi_i(\theta)$ and a scalar θ such that the degrees of freedom,q_i of the human-exoskeleton system are parameterized for $i = 1 \dots 4$.*

5.2 Experimental Setup

5.2.1 Original Plan

Being very relevant for medical exoskeletons the Lower Body AXO suit mentioned in section 3.1.8 was chosen for the experiments. Controllers for walking exists for this exoskeleton, but no controllers for STS-motions exists[1]. The LB-AXO(Shown in Figure 5.1) being a active exoskeleton with encoders the measurement of the joint angles should have been available. However due to software limitations it was not possible in the allotted time(this became clear during the first of two days spent at the University of Gävle where the experiment were to be performed) to improve the code and take the measurement series needed for the project. The choice was then made to use another exoskeleton.

5.2.2 Revised plan

The alternative exoskeleton chosen was the LegX passive exoskeleton3.1.9 this being a passive exoskeleton, means that the joint angles were not readily available and another way of obtaining these measurements was found. Using Inertial measurements units(IMU). It is important to note that the change of experimental setup also changes the end state of the project. If the LB-AXO suit was used then it would be possible to develop a controller and test it on the exoskeleton rig, the Leg-X being a passive exoskeleton precludes this possibility. Thus this project becomes a theoretical exercise in how one would improve

[1] To the knowledge of the author

Figure 5.1: LB-AXO

the movements by introducing actuators/or how a person can try to produce torques in his own body for optimal movements.

5.3 Inertial Sensors

To find trajectories to be improved a test person(measurements of which can be found in table 5.1) wore 4 inertial measurement units(MTw) containing 3D linear accelerometers, 3D-rate gyroscopes, 3D-magnetometers and a barometer[63]. The placement of the sensors on the test person and the orientation of the sensor frames is shown in Figure 5.2.

The test person performed sitting and rising motions in several different configurations, without wearing the exoskeleton, with the exoskeleton

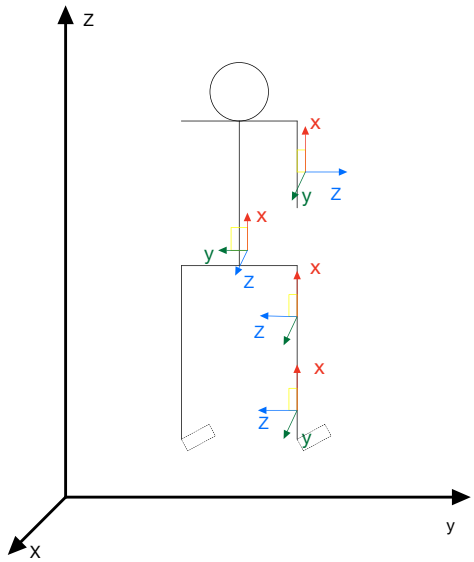

Figure 5.2: The world(G) and sensor(S_i) frames on the test person. The MTw calculates the orientation between the sensor-fixed coordinate system, and an earth-fixed coordinate system, G. By default G is defined as: X positive when pointing to the local magnetic North. Y according to the right handed coordinates(West). Z positive when pointing up [63]

Variable	Value	Unit
Height	1,90	m
Height with shoes	1,92	cm
Weight	110	kg

Table 5.1: Test person measurements

Due to the limited amount of available sensors and the assumed symmetry of the movement(as in [38]) The sensors were placed on the right side of the body, except the sensor

Sensor placement	h_0	h_1	Unit
Medial Lower leg(Shin)	0,33	0,375	m
Medial thigh	0,64	0,685	m
Posterior back(Lower back)	1,22	1,265	m
Lateral Upper arm	1,33	1,375	m

Table 5.2: Sensor heights, where h_0 us the height from the floor to the lowest part of the sensor and h_1 is the height from the floor to the top of the sensor

Parameter	Lower Legs	Upper legs	Torso	Arms
Length(m)	$l_1 = 0.546$	$l_2 = 0.481$	$l_3 = 0.893$	$l_4 = 0.841$
Mass(kg)	$m_1 = 12.54$	$m_2 = 31.152$	$m_3 = 55.44$	$m_4 = 10.868$
Distance to CoM_x	$r_1 = 0.362$	$r_2 = 0.267$	$r_3 = 1.320$	$r_4 = 0.354$
Limb	$a_{1x} = l_1$	$a_{2x} = l_2$	$a_{3x} = l_3$	$a_{4x} = l_4$
dimensions	$a_{1y} = 0.12$	$a_{2y} = 0.1867$	$a_{3y} = 0.19$	$a_{4y} = 0.09$
(m)	$a_{1z} = 0.12$	$a_{2z} = 0.1867$	$a_{3z} = 0.36$	$a_{4z} = 0.09$

Table 5.3: Estimated masses, based on percentages of body weight for each limb of the male subject in [11].Estimated centers of mass, based on *Large male aviator* in [41] scaled up to the height of the test person. Since the trunk, lower leg and arm are made up of more than one segment the combined center of mass was calculated by $\vec{R} = \frac{1}{M}\sum_1^n m_i \vec{r}_i$ found in [9]

on the torso which was placed on the lower back due to the nature of the exoskeleton harness. Since the foot doesn't move in STS-motions there was not placed a sensor there. If more sensors were available then a sensor on the foot, left side forearms and even the head would be interesting to validate the assumptions that the foot doesn't move, that the left and right side move in unison and that the head moves in line with the torso.

5.3.1 Synchronization functions

After the data is gathered there is attempted to find a polynomial of degree $n = 3$ such that the degrees of freedom can be expressed as a function by one of the other ones. The degree of $n = 3$ has been shown to be sufficient in [32] and [38].

$$\begin{aligned} q_1(\theta) &= \phi_1(\theta) = k_{11} + k_{12}\theta + k_{13}\theta^2 + k_{14}\theta^3 \\ q_2(\theta) &= \phi_2(\theta) = \theta \\ q_3(\theta) &= \phi_3(\theta) = k_{31} + k_{32}\theta + k_{33}\theta^2 + k_{34}\theta^3 \\ q_4(\theta) &= \phi_4(\theta) = k_{41} + K_{42}\theta + k_{43}\theta^2 + k_{44}\theta^3 \end{aligned} \tag{5.1}$$

Where

$$\begin{bmatrix} q_1 \\ q_2 \\ q_3 \\ q_4 \end{bmatrix} = \begin{bmatrix} q_{\text{Shank}} \\ q_{\text{Thigh}} \\ q_{\text{Back}} \\ q_{\text{Arm}} \end{bmatrix} \tag{5.2}$$

With the coefficients(k_{ij}) of $\phi_i(\theta)$ found one can find trajectories by solving

$$\begin{aligned} \dot{x_1} &= x_2 \\ \dot{x_2} &= \frac{1}{\alpha(k_{ij}, x_1)} \left[-\beta(k_{ij}, x_1) x_2^2 - \gamma(k_{ij}, x_1) \right] \end{aligned} \tag{5.3}$$

Where $x_1 = q_2$ and $\alpha(\theta), \beta(\theta), \gamma(\theta)$ as defined in (4.39). Here q_2 is used as an example, because it seemed the most promising degree of freedom, any of the others can be chosen with varying degrees of suitability and calculations required. Choosing the passive coordinate often is the least complex from a calculation standpoint.

6

Analysis

6.1 Results

For a degree of freedom to be used as a motion generator, θ it must be monotonic(Either entirely non-increasing or non-decreasing) in time to uniquely define the functions $\phi_i(\theta)$.

Since the joint angles is not directly available it was attempted use the Euler angles instead. If one looks at Figure 6.1 and 6.2 the Thigh sensor seems to be the best candidate. Indeed if one looks at Figure 6.3and 6.4 it looks very promising, but it is not entirely monotonic. The question remains; whether the parts that are not monotonic are due to the motion artifacts, disturbance of the sensor, or are an inherent part of the subjects biomechanics. If one again looks at Figure 6.3 and 6.4 we again can see the "Jump" at $t \approx 1.25$, these recordings are entirely independent and the fact that this appears in both sets of data implies that it part of some "real" part of the movement. If it was due to sensor movement one would expect to find it at "random" time moment. In contrast if we look at Figure 6.3 around $t \approx 2.25$ we see a "dip" that only appears on this Figure and not Figure 6.4

Since the unprocessed data is not monotonic it, can't be used as a motion generator. Any attempt of doing this led to promising values for the knee angle, $q_2 \approx\in [0.4, 1.7]$ congruent with the values in [38] and phase portraits with the periodic orbits, but when substituting back to get for instance the ankle angle (q_1) this lead to values larger than π.

If instead filtering with a Gaussian filter as shown in Figure 6.5 one recovers a monotonic function, but the found coefficients found led to computational stiff equations that couldn't be solved even with Matlab's solvers for stiff ODEs[35]. To be successful in finding the good motion generator further research on methods to process the data is required. Since the trajectories to be controlled were not found, then a controller using the method of VHC cannot be found. To summarize it was not possible to confirm the hypothesis 1 at this time, but with further work this would probably be possible.

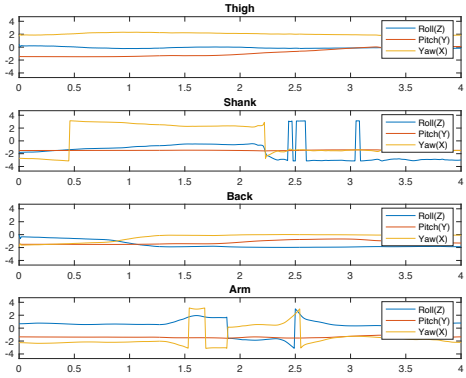

Figure 6.1: Euler Angles when the exoskeleton is not worn during the sitting motion.

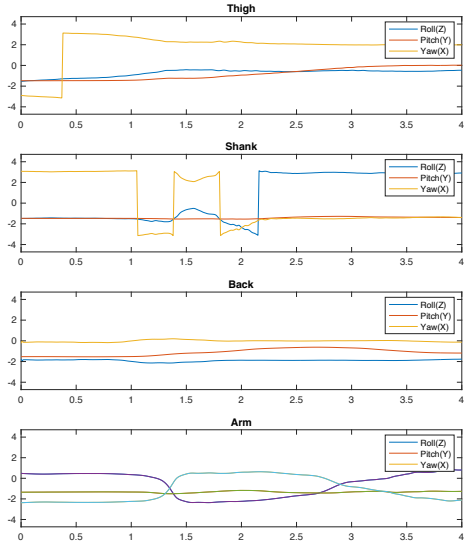

Figure 6.2: Euler Angles when the exoskeleton is worn, but turned off during the sitting motion.

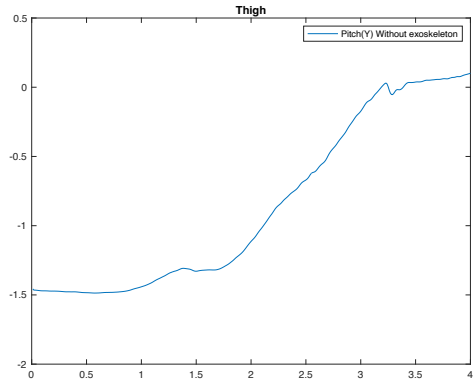

Figure 6.3: The pitch angle at the Thigh from the IMU sensors, without exoskeleton. Notice in particular the motion artifacts and the jump at $t \approx 1.5s$

6.2 Sources of error

6.2.1 Movement of sensor

The MTw Awinda kit normally contains a set of specialized Velcro straps to minimize sensor movement and skin motion artefacts. These straps were missing from the set used and made it necessary to improvise the fastening of the sensors. Strong rubber bands and double-sided tape were used to improvise, but most likely the solution was not optimal as we can see motion artifacts in 6.4.

6.2.2 Time length of movement

The sit-down motions are longer than natural motions for a subject of the test persons age($\approx 3-4$ seconds) compared to the results reported in [38](≈ 0.5 seconds). This was necessary due to the fastening of the sensors, but also for safety when using the Leg-X because the exoskeleton changed the balance point of the user, requiring them to be careful at the end of the motion as to not tip over. Had more time with the exoskeleton been available then it is expected that the time needed to perform the movement world decrease

6.2.3 Number of sensors

At the time of the experiment only 4 IMUs(inertial measurement unit) were available so the choice of sensor placement was limited. The MTw Awinda system supports up to 20 MTw sensors and if more were available, then for instance the foot would be a location to have another sensor. It was assumed that since the foot is not moving during Stand-to-sit motions then it would not be necessary, but during data visualization and manipulation this would have made a lot of the process easier.

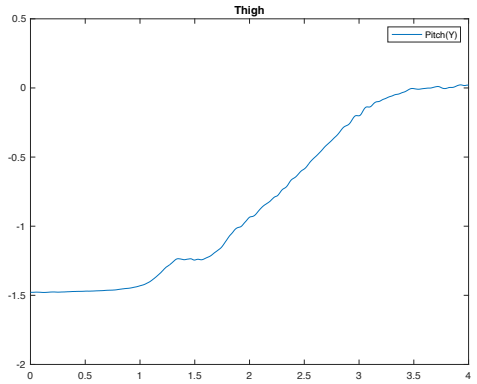

Figure 6.4: The pitch angle at the thigh from the IMU sensors, when the exoskeleton is worn and assistance is turned off. Notice in particular the motion artifacts and the jump at $t \approx 1.5s$ which is very similar to the case when the exoskeleton is worn

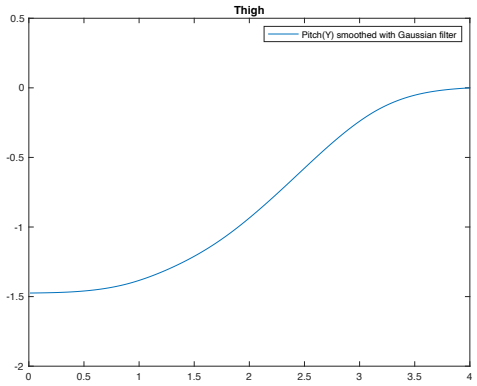

Figure 6.5: The data of Figure 6.4 smoothed with a Gaussian filter. This is monotonic, but one can't guarantee that this if fully representative of the movement itself.

6.2.4 World frame orientation

The direction of magnetic North was not measured at the time of the experiments, meaning that the orientation of the World frame x-axis was not known. This means that one can not use this frame to find the orientation directly.

6.2.5 Magnetic Distortion

Xsens Awinda Mtw uses a Kalman filter[44][63] specifically named XKF3hm(*Xsens Kalman Filter 3 DOF for Human Motion 6*) to combine 3D inertial data and 3d magnetometer data to find the orientation of the sensor in regards to the world frame G. In particular it uses the magnetometer data in the beginning of recording data to get the heading. Therefore the results are sensitive to magnetic disturbances in the area. Areas with a magnetic norm

variation within ± 0.2. It is therefore advisable to check the magnetic norm of the environment, but this was not done at the time of the experiment leading to uncertainty in the results. By visual inspection no obvious sources of magnetic disturbances where found.

6.3 Potential improvements

6.3.1 World frame orientation

Magnetic North should be measured at the start of the experiment and all test series should be aligned with this as the x-axis. This would align the world frame with the body frame. This would ease visualization and calculation efforts.

If the experiments were to be done anew then magnetic north should be measured beforehand and the test person should be lined up facing in that direction for all test series.

6.3.2 Object orientation frame

As shown in figure 5.2 the sensor frames(S) z-axis does not align with the world frame(G) z-axis to simplify the calculations the output data could be expressed in the orientation between a known Object Frame(O) and World Frame(G) rather than between S-frame and G by applying the following relation

$$R_{GO} = R_{GS} \left(R_{OS}\right)^T \tag{6.1}$$

where

$$R_{OS} = R_y(\theta) = \begin{bmatrix} \cos(\theta) & 0 & \sin(\theta) \\ 0 & 1 & 0 \\ -\sin(\theta) & 0 & \cos(\theta) \end{bmatrix} \Bigg|_{\theta=-\frac{\pi}{2}} = \begin{bmatrix} 0 & 0 & -1 \\ 0 & 1 & 0 \\ 1 & 0 & 0 \end{bmatrix} \tag{6.2}$$

It should be note that this is an example orientation change. In this experiment one would

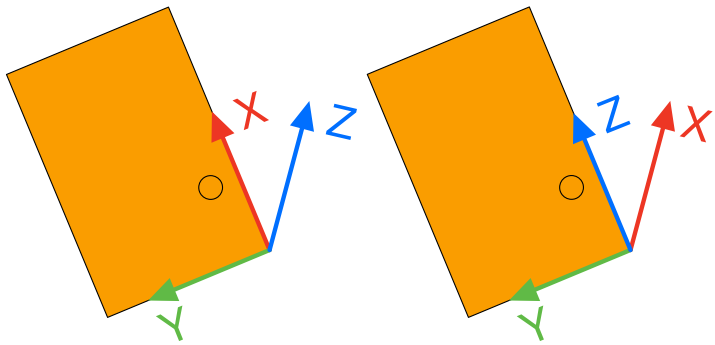

(a) Sensor Frame(S)

(b) Object Frame(O) obtained by a rotation of S by $\frac{\pi}{2}$ about the y-axis

Figure 6.6: Relation between Sensor frame(S) and Object frame(O)

need different rotation matrix for almost all of the sensors, given that only the thigh and shank frames are aligned.

6.3.3 Using more sophisticated software

For this experiment the free software Mt Manager[64] made by Xsens was used, it is definitely adequate, but more sophisticated paid software exists. From the same developer we have the MVN systems, MVN Animate used for motion capture for 3D animation and MVN Analyze for Human motion analysis/biomechanics and related fields[34]. This software requires the users to input the dimensions of the subject beforehand and each sensor has an ID corresponding to a particular body subject, but this along with calibration and built in biomechanical model means that the readings are immune to magnetic distortion and the system can output the joint angles of the body segment(limbs) directly [47]. The movement can also be viewed with a humanoid avatar greatly helping in movement classification after the fact.

6.3.4 Methods of obtaining joint angles by way of IMUs

The use of IMUs for measuring joint angles is a area of keen research interest, and new research has been published on the field during the work on this thesis like [68] and [4]. The use of IMUs for biomechanical analysis is of popular because it avoids many common problems associated with other ways of measuring joint angles. Optical methods require proper lighting conditions, optical markers , a proper camera setup and requires the test person to be stationary(for walking, a treadmill is needed)[22][68]. Magnetic resonance systems based imaging methods [19] requires a clinical setup which limits utility in many situations.

Using IMUs avoids these problems, but introduces other challenges like calibration and when taking measurements over longer time periods, sensor drift. There have been developed for handling these problems as:

Self-Aligned Method of IMU-Based 3-DoF Lower-Limb Joint Angle Estimation [68] presents a method to obtain the lower leg joint angles of a subject without the need of calibration beforehand. They achieve good accuracy compared to other methods and does not necessitate calibration. Different methods of calibration are compared in [23].

OpenSense: An open-source toolbox for inertial-measurement-unit-based Open Access measurement of lower extremity kinematics over long durations [4] Developed a toolkit for improving the accuracy of IMUs over longer time periods(more than a minute) avoiding drift. The results were validated by optical methods. The methods still requires calibration.

7

Conclusion

> "Quaternions came from Hamilton after his really good work had been done, and though beautifully ingenious, have been an unmixed evil to those who have touched them in any way." - Lord Kelvin[58]

This thesis aimed to find control strategies for exoskeletons for humans use. If one were to look back at the tasks set forth in 2.1 the most central objectives were:

1. Develop a control system for a human-exoskeleton system

2. Test the developed control system on a given exoskeleton setup.

Based on a results and analysis it cannot be concluded on such an optimal control input. The lack of results indicate that more work must be done. It also shows the challenges in adapting results on a given setup as in [32] and [38] to a new setup, especially when having to rely on sensors and technology that was unknown to the writer at time of the experiment. It also shows the difficulty when used to work with regular joint angles and then trying to visualize and work with motions in $3D$-space represented by Euler-angles or Quaternions.

7.1 Future work and continuation

7.1.1 Original Setup

If the original experimental setup(Lower Body AXO) was to be used again it is expected that one would need some more time to be familiarized with the exoskeleton and the code base. The exoskeleton is fully functional, but new code would have to be written to access the joint angles. The exoskeleton itself has all the functionality and connections to access the angles in practice. It should be noted that this particular exoskeleton was bolted to a treadmill, but this is a trivial concern.

7.1.2 Revised plan

If using the revised plan further research into methods of using IMUs for body kinematics is required, some improvements are already mentioned in 6.3. Further more it must be investigated if the anomalies are a property of the movement or one of the error sources.

7.1.3 Continuation

For either setup the next step is to design a controller to stabilize the trajectories found through the virtual holonomic constraints.

If such a controller is found then for the Lower Body AXO it can then by tested with a user operating it.

If one were to proceed with the Leg-X suit, then it is not realistic to validate in this way, but one could see if the calculated necessary torques at knee, hip and arms are realistic for a human to be able to produce. Not only in magnitude, but in change of torque in time.

Bibliography

[1] AAL Association. Axo-suit, Dec 2018.

[2] AAL Association. Exo-legs, Dec 2018.

[3] D. Accoto, F. Sergi, N. L. Tagliamonte, G. Carpino, A. Sudano, and E. Guglielmelli. Robomorphism: A nonanthropomorphic wearable robot. *IEEE Robotics &; Automation Magazine*, 21(4):45–55, 2014.

[4] M. Al Borno, J. O'Day, V. Ibarra, J. Dunne, A. Seth, A. Habib, C. Ong, J. Hicks, S. Uhlrich, S. Delp, and et al. Opensense: An open-source toolbox for inertial-measurement-unit-based measurement of lower extremity kinematics over long durations. *Journal of NeuroEngineering and Rehabilitation*, 19(1), 2022.

[5] B. D. Anderson and J. B. Moore. *Optimal control: Linear quadratic methods*. Dover Publications, 2007.

[6] R. G. Baldovino and R. S. Jamisola. A survey in the different designs and control systems of powered exoskeleton for lower extremities. *Journal of Mechanical Engineering and Biomechanics*, 1(4):103–115, 2017.

[7] C.-T. Chen. *Controllability and Observability*, chapter 6, pages 176–179. Oxford University Press, 3 edition, 1999.

[8] S. Christensen, S. Rafique, and S. Bai. Design of a powered full-body exoskeleton for physical assistance of elderly people. *International Journal of Advanced Robotic Systems*, 18(6):172988142110535, 2021.

[9] D. Cline, M. Sarkis, and D. Cline. *Review of Newtonian mechanics*, page 13–13. University of Rochester River Campus Libraries, 3 edition, 2021.

[10] Collins English Dictionary. Definition of dystrophy. In *collinsdictionary.com*. HarperCollins Publishers, 2022.

[11] P. de Leva. Adjustments to Zatsiorsky-Seluyanov's segment inertia parameters. *Journal of Biomechanics*, 29(9):1223–1230, 1996.

[12] B. R. Fick and J. B. Makinson. Hardiman I prototype, Dec 2012.

[13] S. Gusev, S. Johansson, B. Kågström, A. Shiriaev, and A. Varga. A numerical evaluation of solvers for the periodic riccati differential equation. *BIT Numerical Mathematics*, 50(2):301–329, 2010.

[14] S. V. Gusev, A. S. Shiriaev, and L. B. Freidovich. Lmi approach for solving periodic matrix riccati equation. *IFAC Proceedings Volumes*, 40(14):254–256, 2007.

[15] S. V. Gusev, A. S. Shiriaev, and L. B. Freidovich. Sdp-based approximation of stabilising solutions for periodic matrix riccati differential equations. *International Journal of Control*, 89(7):1396–1405, 2016.

[16] F. Hapgood. When robots live among us, May 2008.

[17] O. Harib, A. Hereid, A. Agrawal, T. Gurriet, S. Finet, G. Boeris, A. Duburcq, M. E. Mungai, M. Masselin, A. D. Ames, and et al. Feedback control of an exoskeleton for paraplegics: Toward robustly stable, hands-free dynamic walking. *IEEE Control Systems*, 38(6):61–87, Nov 2018.

[18] P. Ioannou and J. Sun. *Robust Adaptive Control*. Dover Publications, 2013.

[19] H. Kainz, L. Modenese, D. Lloyd, S. Maine, H. Walsh, and C. Carty. Joint kinematic calculation based on clinical direct kinematic versus inverse kinematic gait models. *Journal of Biomechanics*, 49(9):1658–1669, Jun 2016.

[20] R. Kalman. Contributions to the theory of optimal control. *Boletin de la Sociedad Matematica Mexicana*, 5(102), 1960.

[21] H. K. Khahil. *Nonlinear Systems*. Pearson Education Limited, 3 edition, 2015. Compiled from: Nonlinear systems, Third Edition, Hassan K. Khalil.

[22] H. Lamine, S. Bennour, M. Laribi, L. Romdhane, and S. Zaghloul. Evaluation of calibrated kinect gait kinematics using a vicon motion capture system. *Computer Methods in Biomechanics and Biomedical Engineering*, 20(sup1), 2017.

[23] J. Lebleu, T. Gosseye, C. Detrembleur, P. Mahaudens, O. Cartiaux, and M. Penta. Lower limb kinematics using inertial sensors during locomotion: Accuracy and reproducibility of joint angle calculations with different sensor-to-segment calibrations. *Sensors*, 20(3):715, 2020.

[24] G. Leonov. Generalization of the andronov–vitt theorem. *Regular and Chaotic Dynamics*, 11(2):281–289, 2006.

[25] D. Lovely. Signals and signal processing for myoelectric control. In A. Muzumdar, editor, *Powered upper limb prostheses control, implementation and clinical application*, page 35–42. Springer Berlin, 2014.

[26] B. J. Makinson. Research and development prototype for machine augmentation of human strength and endurance. hardiman i project. Technical report, GENERAL ELECTRIC COMPANY CORPORATE RESEARCH AND DEVELOPMENT, 1971.

[27] N. Masud. *About physical human robotic interaction for assistive exoskeletons*. PhD thesis, 2021.

[28] Merriam-Webster. Anthropomorphic definition & meaning, Feb 2022.

[29] Merriam-Webster. Exo- definition & meaning, Feb 2022.

[30] Merriam-Webster. Exoskeleton definition & meaning, Feb 2022.

[31] Merriam-Webster. Paraplegia definition & meaning, May 2022.

[32] U. Mettin, P. X. L. Hera, L. B. Freidovich, A. S. Shiriaev, and J. Helbo. Motion planning for humanoid robots based on virtual constraints extracted from recorded human movements. *Intelligent Service Robotics*, 1(4):289–301, 2008.

[33] M. E. Mungai and J. W. Grizzle. Feedback control design for robust comfortable sit-to-stand motions of 3d lower-limb exoskeletons. *IEEE Access*, 9:122–161, Jan 2021.

[34] N. N. Mvn analyze, Nov 2019.

[35] N. N. Solve stiff odes, 2022.

[36] J. Nestruev and J. Nestruev. *Cutoff and Other Special Smooth Functions on $\mathcal{R}^n$*, page 13–18. Springer Nature Switzerland, 2 edition, 2020.

[37] N,N. CYBERDYNE obtained marketing clearance from U.S. FDA for Medical HAL as a medical device. *News*, Dec 2017.

[38] S. Pchelkin, A. S. Shiriaev, L. B. Freidovich, U. Mettin, S. V. Gusev, W. Kwon, and L. Paramonov. A dynamic human motion: coordination analysis. *Biological Cybernetics*, 109(1):47–62, 2014.

[39] M. V. Pillai, L. Van Engelhoven, and H. Kazerooni. Evaluation of a lower leg support exoskeleton on floor and below hip height panel work. *Human Factors: The Journal of the Human Factors and Ergonomics Society*, 62(3):489–500, 2020.

[40] J. Pratt, B. Krupp, C. Morse, and S. Collins. The roboknee: An exoskeleton for enhancing strength and endurance during walking. *IEEE International Conference on Robotics and Automation, 2004. Proceedings. ICRA '04. 2004*, page 2430–2435, Apr 2004.

[41] A. R. Project. *Military Male aviators*, volume 1. Anthropology Research Project, 1988.

[42] S. Puntanen and G. P. H. Styan. *Historical Introduction: Issai Schur and the Early Development of the Schur Complement*, page 1–15. Springer, 2005.

[43] Rex Bionics. Product information, Dec 2019.

[44] D. Roetenberg. *Inertial and magnetic sensing of human motion*. PhD thesis, 2006.

[45] W. Rudin. *Integration on Product Spaces*, page 144–144. McGraw-Hill Book Company, 3 edition, 1987. International Edition.

[46] Y. Sankai. Hal: Hybrid assistive limb based on cybernics. *Springer Tracts in Advanced Robotics*, page 25–34, 2010.

[47] M. Schepers, M. Giuberti, and G. Bellusci. Xsens MVN: Consistent tracking of human motion using inertial sensing, 03 2018.

[48] A. Shiriaev. Introduction: Tools for analysis of second order systems, 2020. ©Anton Shiriaev & Robotikum freeware. Underactuated systems & DM. 2020: Lecture 2.

[49] A. Shiriaev, L. Freidovich, and S. Gusev. Transverse linearization for controlled mechanical systems with several passive degrees of freedom. *IEEE Transactions on Automatic Control*, 55(4):893–906, 2010.

[50] A. Shiriaev, L. Freidovich, and I. Manchester. Can we make a robot ballerina perform a pirouette? orbital stabilization of periodic motions of underactuated mechanical systems. *Annual Reviews in Control*, 32(2):200–211, Dec 2008.

[51] A. Shiriaev, J. Perram, and C. Canudas-De-Wit. Constructive tool for orbital stabilization of underactuated nonlinear systems: virtual constraints approach. *IEEE Transactions on Automatic Control*, 50(8):1164–1176, 2005.

[52] A. Shiriaev, A. Robertsson, J. Perram, and A. Sandberg. Periodic motion planning for virtually constrained Euler–Lagrange systems. *Systems & Control Letters*, 55(11):900–907, 2006.

[53] M. Spong. Partial feedback linearization of underactuated mechanical systems. In *Proceedings of IEEE/RSJ International Conference on Intelligent Robots and Systems (IROS'94)*, volume 1, pages 314–321 vol.1, 1994.

[54] M. W. Spong, S. Hutchinson, and M. Vidyasagar. *Geometric Nonlinear Control*, page 362–363. John Wiley &; Sons, 2006.

[55] Stablenode. Poincare-bendixson illustration, 2005. Stablenode, CC BY-SA 3.0 `https://creativecommons.org/licenses/by-sa/3.0`, via Wikimedia Commons.

[56] K. Suzuki, G. Mito, H. Kawamoto, Y. Hasegawa, and Y. Sankai. Intention-based walking support for paraplegia patients with robot suit hal. *Advanced Robotics*, 21(12):1441–1469, 2007.

[57] R. Tedrake. *Underactuated Robotics*. MIT, 2022.

[58] S. P. Thomson. *The Life of William Thomson, Baron Kelvin of Largs*, volume 2. Macmillan and Co., 1910.

[59] A. Varga. On solving periodic riccati equations. *Numerical Linear Algebra with Applications*, 15(9):809–835, Aug 2008.

[60] G. S. Virk, U. Haider, I. N. Indrawibawa, R. K. Thekkeparampumadom, and N. Masud. 17th International Conference on Climbing and Walking Robots and the Support Technologies for Mobile Machines. In *Mobile Service Robotics*, page 85–92. World Scientific, 2014.

[61] M. Vukobratović. When were active exoskeletons actually born? *International Journal of Humanoid Robotics*, 04(03):459–486, 2007.

[62] M. Vukobratović, B. Borovac, D. Surla, and D. Stokić. *Biped Locomotion*. Communications and Control Engineering Series. Springer, Berlin, Heidelberg, 1 edition, 1990.

[63] Xsens Technologies B.V. *MTw Awinda User Manual*. Xsens, Enschede, The Netherlands, Document MW0502P, Revision L, 3 May 2018 edition, 2018.

[64] Xsens Technologies B.V. *MT Manager User Manual*. Xsens, Enschede, The Netherlands, Document MT0605P, Revision 2020.A, June 2020 edition, 2020.

[65] N. Yagn. Apparatus for facilitating walking,running,and jumping, Jan 1890. US Patent 420, 179.

[66] V. A. Yakubovich. Linear-quadratic optimization problem and the frequency theorem for periodic systems. ii. *Siberian Mathematical Journal*, 31(6):1027–1039, 1991.

[67] T. Yan, M. Cempini, C. M. Oddo, and N. Vitiello. Review of assistive strategies in powered lower-limb orthoses and exoskeletons. *Robotics and Autonomous Systems*, 64:120–136, 2015.

[68] C. Yi, B. Wei, Z. Ding, C. Yang, Z. Chen, and F. Jiang. A self-aligned method of imu-based 3-dof lower-limb joint angle estimation. *IEEE Transactions on Instrumentation and Measurement*, 71:1–10, Jul 2022.

[69] A. Zoss, H. Kazerooni, and A. Chu. On the mechanical design of the berkeley lower extremity exoskeleton (bleex). In *2005 IEEE/RSJ International Conference on Intelligent Robots and Systems*, pages 3465–3472, 2005.

[70] A. Zoss, H. Kazerooni, and A. Chu. Biomechanical design of the berkeley lower extremity exoskeleton (bleex). *IEEE/ASME Transactions on Mechatronics*, 11(2):128–138, 2006.

A

Theorems, definitions and lemmas

A.1 Theorems

Theorem A.1.1 (Newton-Leibniz Formula[45][1])**.** *Let $f(x)$ be a function defined on some compact interval $[a, b]$ in $\mathcal{R}^1$*

$$F(b) - F(a) = \int_a^b f(x)dx \quad a \leq x \leq b \tag{A.1}$$

A.2 Lemmas

Lemma A.2.1 (Hadamard's Lemma[36])**.** *Any smooth function f in a starlike neighborhood of a point z is representable in the form*

$$f(x) = f(z) + \sum_{i=1}^{n}(x_1 - z_i)g_i(x), \tag{A.2}$$

where g_i are smooth functions.

A.3 Definitions

Definition A.3.1 (Fundamental matrix)**.** Consider

$$\dot{x} = A(t)x(t). \tag{A.3}$$

Where $A(t) \in \mathcal{R}^{n\times n}$ with continuous function of t as its entries. Then for every initial state $x_i(t_0)$ there exist a unique solution $x_i(t)$, for $i = 1, 2, \ldots, n$. If one arranges these n solutions as $X = [x_1 x_2 \ldots x_n] \in \mathcal{R}^{n\times n}$ because every x_i satifies (A.3) we have

$$\dot{X} = A(t)X(t) \tag{A.4}$$

[1] Also known as the *The Fundamental Theorem of Calculus*

if $X(t_0)$ is nonsingular then $X(t)$ is called the *fundamental matrix* of (A.3)

Definition A.3.2 (State transition Matrix [7])**.** Let $X(t)$ be any fundamental matrix of (A.3) Then

$$\mathbf{\Phi}(t, t_0) := X(t)X^{-1}(t_0) \tag{A.5}$$

is called the *state transition matrix* of (A.3). The state transition matrix is also the unique solution of

$$\frac{\partial}{\partial t}\mathbf{\Phi}(t, t_0) = A(t)\mathbf{\Phi}(t, t_0) \tag{A.6}$$

with the initial condition $\mathbf{\Phi}(\mathbf{t_0}, \mathbf{t_0}) = I$

B

Proofs

B.1 Proof of A.2.1

Hadamard's Lemma[36]. Consider the function

$$\varphi(t) = f(x + (x - z)t)$$

Where $\varphi(0) = f(x)$ and $\varphi(1) = f(x)$, by the Newton-Leibniz Formula Theorem A.1.1

$$\begin{aligned}\varphi(1) - \varphi(0) = \int_0^1 \frac{d\varphi}{dt} dt = \int_0^1 \sum_{i=1}^{n} \frac{\partial f}{\partial x_i}(z + (x_i - z_i)t)(x_i - z_i)dt \\ = \sum_{i=1}^{n}(x_i - z_i) \int_0^1 \frac{\partial f}{\partial x_i}(z + (x_i - z_i)t)dt\end{aligned}$$

Since the functions

$$g_i = \int_0^1 \frac{\partial f}{\partial x_i}(z + (x_i - z_i)t)dt$$

are smooth, this concludes the proof □

B.2 Proof of 4.6.1

Based on [51]

Proof. Consider the system

$$\alpha(\theta)\ddot{\theta} + \beta(\theta)\dot{\theta}^2 + \gamma(\theta) = 0 \tag{B.1}$$

if one introduces a variable $Y := \dot{\theta}^2$ then

$$\frac{dY}{dt} = \frac{d}{dt}\left(\dot{\theta}^2(t)\right) = 2\dot{\theta}\ddot{\theta} \tag{B.2}$$

and by the chain rule

$$\frac{dY}{dt} = \frac{dY}{d\theta}\frac{d\theta}{dt} = \frac{dY}{d\theta}\dot{\theta}. \tag{B.3}$$

thus along a solution of (B.1) this identity holds:

$$\ddot{\theta} = \frac{1}{2}\frac{dY}{d\theta} \tag{B.4}$$

and one can rewrite (B.1) as

$$\alpha(\theta)\frac{1}{2}\frac{dY}{d\theta} + \beta(\theta)Y + \gamma(\theta) = 0 \tag{B.5}$$

This new differential is linear with θ as the new independent variable. Let $\alpha(\theta) \neq 0$ along a solution $(\theta^*(t), \dot{\theta}^*(t))$ Then one can rewrite (B.5) as

$$\frac{d}{d\theta}Y + \frac{2\beta(\theta)}{\alpha(\theta)} + \frac{2\gamma(\theta)}{\alpha(\theta)} = 0 \tag{B.6}$$

This equation has the general solution

$$Y(\theta) = \psi(\theta_0, \theta)Y(\theta_0) - \psi(\theta_0, \theta)\int_{\theta_0}^{\theta} \psi(s, \theta_0)\frac{2\gamma(s)}{\alpha(s)}ds \tag{B.7}$$

Where $\psi(\cdot)$ is as defined in (4.41). (B.7) means that

$$I(\theta, \dot{\theta}, \theta_0, \dot{\theta}_0) = \dot{\theta}(t)^2 - Y(\theta(t)) \tag{B.8}$$

and along the solution $(\theta^*(t), \dot{\theta}^*(t))$

$$I(\theta^*, \dot{\theta}^*, \theta_0, \dot{\theta}_0) = \dot{\theta}^*(t)^2 - Y(\theta(t)^*) \equiv 0 \tag{B.9}$$

[1] □

B.3 Proof of 4.6.2

Based on [51]

Proof. By the chain-rule:

$$\frac{d}{dt}I = \frac{\partial I}{\partial \theta}\dot{\theta} + \frac{\partial I}{\partial \dot{\theta}}\ddot{\theta} \tag{B.10}$$

Where $I(\theta, \dot{\theta}, \theta_0, \dot{\theta}_0)$ as defined in B.8.

$$\frac{\partial I}{\partial \dot{\theta}} = 2\dot{\theta} \quad \text{and} \quad \frac{\partial I}{\partial \theta} = \frac{2\gamma(\theta)}{\alpha(\theta)} - \frac{2\beta(\theta)}{\alpha(\theta)}\left[I - \dot{\theta}^2\right] \tag{B.11}$$

[1] The proof for the case when $\alpha(\theta) = 0$ is not relevant for this thesis and is thus omitted.

This means that

$$\begin{aligned}\dot{I} &= \left\{ \frac{2\gamma(\theta)}{\alpha(\theta)} - \frac{2\beta(\theta)}{\alpha(\theta)} \left[I - \dot{\theta}^2 \right] \right\} \dot{\theta} + 2\dot{\theta} \left\{ \frac{W - \beta(\theta)\dot{\theta}^2 - \gamma(\theta)}{\alpha(\theta)} \right\} \\ &= \frac{2\dot{\theta}}{\alpha(\theta)} \{ W - \beta(\theta) I \}\end{aligned} \tag{B.12}$$

□

B.4 Proof of 4.7.1

Proof. $\mathbf{W}_c(t_0, t_1)$nonsingular $\Rightarrow$ $(A(t), b(t))$ controllable:

$$x(t_1) = \mathbf{\Phi}(t_1, t_0)x_0 + \int_{t_0}^{t_1} \mathbf{\Phi}(t_1, \tau)b(\tau)u(\tau)d\tau \tag{B.13}$$

If we choose the input that will change the state of the system from x_0 to x_1 as

$$u(t) = -b(t)^T \mathbf{\Phi}(t_1, t)^T \mathbf{W}_c^{-1}(t_0, t_1)[\mathbf{\Phi}(t_1, t_0)x_0 - x_1] \tag{B.14}$$

and substitute it into (B.13) gives us

$$\begin{aligned} x(t_1) &= \mathbf{\Phi}(t_1, t_0)x_0 \\ &\quad - \int_{t_0}^{t_1} \mathbf{\Phi}(t_1, \tau)b(\tau)b(\tau)^T \mathbf{\Phi}(t_1, \tau)^T \mathbf{W}_c^{-1}(t_0, t_1)[\mathbf{\Phi}(t_1, t_0)x_0 - x_1]d\tau \\ &= \mathbf{\Phi}(t_1, t_0)x_0 \\ &\quad - \left[\int_{t_0}^{t_1} \mathbf{\Phi}(t_1, \tau)b(\tau)b(t)^T \mathbf{\Phi}(t_1, t)^T d\tau \right] \mathbf{W}_c^{-1}(t_0, t_1)[\mathbf{\Phi}(t_1, t_0)x_0 - x_1] \\ &= \mathbf{\Phi}(t_1, t_0)x_0 - \mathbf{W}_c(t_0, t_1)\mathbf{W}_c^{-1}(t_0, t_1)[\mathbf{\Phi}(t_1, t_0)x_0 - x_1] = x_1 \end{aligned} \tag{B.15}$$

Thus if $\mathbf{W}_c$ is nonsingular then $(A(t), b(t))$ is controllable. □

Proof. $(A(t), b(t))$ controllable $\Rightarrow$ $\mathbf{W}_c(t_0, t_1)$ nonsingular: Suppose (4.65) is controllable at t_0, but $\mathbf{W}_c$ is singular or, positive semidefinite, for all $t_1 > t_0$. Then there exist $0 \neq v \in \mathcal{R}^n$ such that@

$$\begin{aligned} v^T \mathbf{W}_c(t_0, t_1)v &= \int_{t_0}^{t_1} v^T \mathbf{\Phi}(t_1, \tau)b(\tau)b(\tau)^T \mathbf{\Phi}(t_1, \tau)^T v d\tau \\ &= \int_{t_0}^{t_1} \| b(\tau)^T \mathbf{\Phi}(t_1, \tau)v \|^2 d\tau = 0 \end{aligned}$$

Thus

$$v^T \mathbf{\Phi}(t_1, \tau)b(\tau) \equiv 0 \quad \text{or} \quad b(\tau)^T \mathbf{\Phi}(t_1, \tau)^T v \equiv 0 \quad \forall \tau \in [t_0, t_1] \tag{B.16}$$

Since (4.65) is controllable then there exists an input that transitions the system from $x_0 = \mathbf{\Phi}(t_0, t_1)v$ at t_0 to $x_1(t_1) = 0$, Inserting this into (B.15) and multiplying it with v^T yields

$$\begin{aligned} 0 &= v^T \mathbf{\Phi}(t_1, t_0)\mathbf{\Phi}(t_0, t_1)v + v^T \int_{t_0}^{t_1} \mathbf{\Phi}(t_1, \tau)b(\tau)u(\tau)d\tau \\ &= v^T Iv + \int_{t_0}^{t_1} v^T \mathbf{\Phi}(t_1, \tau)b(\tau)u(\tau)d\tau \\ &= \|v\|^2 + \int_{t_0}^{t_1} \left[v^T \mathbf{\Phi}(t_1, \tau)b(\tau)\right] u(\tau)d\tau = \|v\|^2 \Rightarrow v = 0 \end{aligned} \tag{B.17}$$

Since we assumed that $v \neq 0$ then we have a contradiction. This means that if $(A(t), b(t))$ controllable then $\mathbf{W}_c$ is nonsingular. □

C

Specialization project report

Developing new abilities for humanoid robots

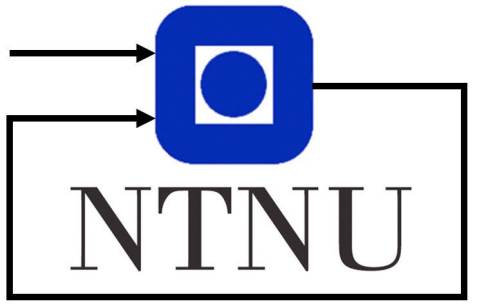

Author:
Vebjørn Steinsholt

Supervisor:
Anton Shiriaev

Specialization project
Department of Engineering Cybernetics
Norwegian University of Science and Technology
September 14, 2022

Summary

It was attempted to control the motion of an inverted pendulum on a cart, this was not achieved. The paper will discuss reasons why, improvements and further work.

Preface

The work presented in this report is the result of work on TTK4550 - Engineering Cybernetics, Specialization Project, at The Norwegian University of Science and Technology. The purpose of the work is:

> The student will specialize in selected area based on scientific methods, collect supplementary information based on literature search and other sources and combine this with own knowledge into a project report.

[1]

I would like to thank my supervisor Professor Anton Shiriaev for helping me and for his work in teaching the course TTK6. I do not think I have learned so much in such a short time ever.

Vebjørn Steinsholt
Trondheim, September 14, 2022

[1] https://www.ntnu.edu/studies/courses/TTK4550

Table of Contents

Summary i

Preface ii

List of Tables v

List of Figures vii

Abbreviations ix

Nomenclature xi

1 Introduction 1
- 1.1 Motivation . . . 1
- 1.2 Scope . . . 1
- 1.3 Tasks . . . 2
- 1.4 Structure . . . 2

2 Literature Review 3
- 2.1 Underactuated systems . . . 3
- 2.2 Humanoid Robots . . . 4

3 Basic Theory 5
- 3.1 Underactuated systems . . . 5
- 3.2 System dynamics . . . 5
- 3.3 Motion Generator . . . 7
- 3.4 Transverse Linearization . . . 8
- 3.5 Linear-Quadratic Regulator . . . 9

4 Experiment 11

5 Analysis **15**
5.1 Results 15
5.2 Sources of error 15
5.3 Potential improvements 15

6 Conclusion **17**
6.1 Future work and continuation 17

Bibliography **19**

Appendix **22**

List of Tables

4.1 Experimental Parameters 11
4.2 Boundary Conditions 11
4.3 Coefficients for the synchronization function $\phi(\theta)$. 13

List of Figures

2.1 Hardiman I prototype, GENERAL ELECTRIC CO SCHENECTADY NY SPECIALTY MATERIALS HANDLING PRODUCTS OPERATION, Public domain, via Wikimedia Commons(Fick and Makinson, 2012) 4

3.1 A cart of mass M, with a point-mass, m. The pendulum makes an angle θ with the vertical axis 6

4.1 Phase plot for the $\alpha\beta\gamma$-system 12
4.2 The most promising solution $\theta^*(t)$ with phase portrait, $\alpha(\theta)$ plotted with $\dot{\theta^*}(t)$ and the force($f(\theta(t))$) applied to the cart to have that trajectory. . . 12

6.1 A: A solution $\theta^*(t)$ with phase portrait, $\alpha(\theta)$ plotted with $\dot{\theta^*}(t)$ and the force($f(\theta(t))$) applied to the cart to have that trajectory. 22
6.2 The most promising solution $\theta^*(t)$ with phase portrait, $\alpha(\theta)$ plotted with $\dot{\theta^*}(t)$ and the force($f(\theta(t))$) applied to the cart to have that trajectory. . . 23
6.3 B: A solution $\theta^*(t)$ with phase portrait, $\alpha(\theta)$ plotted with $\dot{\theta^*}(t)$ and the force($f(\theta(t))$) applied to the cart to have that trajectory. 24
6.4 C: A solution $\theta^*(t)$ with phase portrait, $\alpha(\theta)$ plotted with $\dot{\theta^*}(t)$ and the force($f(\theta(t))$) applied to the cart to have that trajectory. 25
6.5 D: A solution $\theta^*(t)$ with phase portrait, $\alpha(\theta)$ plotted with $\dot{\theta^*}(t)$ and the force($f(\theta(t))$) applied to the cart to have that trajectory. 26
6.6 E: A solution $\theta^*(t)$ with phase portrait, $\alpha(\theta)$ plotted with $\dot{\theta^*}(t)$ and the force($f(\theta(t))$) applied to the cart to have that trajectory. 27

Abbreviations

LQR	=	Linear–quadratic regulator
PRDE	=	Periodic Ricatti Differential Equation
DOF	=	Degrees of freedom
wrt	=	With regards to
i.e	=	*id est* = that is

Nomenclature

Symbol		Definition
x	=	Coordinate of the cart on the world x-axis
θ	=	Angle between the cart body y-axis and the pendulum
$\dot{x}$	=	$\frac{dx}{dt}$, time derivative of x
$\dot{\theta}$	=	$\frac{d\theta}{dt}$, time derivative of θ
$\ddot{x}$	=	$\frac{d^2x}{dt^2}$, second time derivative of x
$\ddot{\theta}$	=	$\frac{d^2\theta}{dt^2}$, time derivative of θ
v_i	=	Velocity of body i
m	=	Mass of pendulum
M	=	Mass of cart
$\frac{\partial}{\partial x}$	=	Partial derivative with regards to coordinate x
f	=	Force applied to cart
$\mathcal{K}$	=	Total kinetic energy of system
$\mathcal{P}$	=	Total potential energy of system
$\mathcal{L}$	=	Lagrangian
$\phi(\theta)$	=	Motion generator/Synchronization function
$\alpha\beta\gamma$-equation	=	$\alpha\ddot{\theta} + \beta(\theta)\dot{\theta}^2 + \gamma(\theta) = 0$
k_i	=	Coefficients of the polynomial chosen for $\phi(\theta)$
$x_{i\perp}$	=	i-th transverse coordinate
I	=	Integral of motion
$K(t)$	=	LQR-gain for the input $v(t) = K(t)x_\perp(t)$ to the linearised system
Q	=	Weight on deviation from states in LQR-control
R	=	Weight on use of control action in LQR-control
$P(t) = P(t+T) = P(t)^T$, $\forall t \in [0, T]$	=	Solution of the periodic Ricatti equation

Chapter 1

Introduction

1.1 Motivation

> "Then you don't remember a world without robots. There was a time when humanity faced the universe alone and without a friend."(Asimov, 2008)

Robots are and have been a big help in various different industries and situations. Formerly relegated to industry and heavy machinery, now they are finding more and more places in our daily lives, from food processing to exoskeletons. In scenarios where they are to be used in aiding a human it is important to have in mind that they do not move like us. For instance they may be heavy, be able to generate more torque at the joints or synchronize their limbs in a different way. An important distinction between us is that a human may be weakly actuated in some joints to such a degree that we may model them as underactuated. Therefore it might be necessary to model the robot mimicking a human as underactuated as well. This project will be a discussion on how to make a robot move to a human specification.

When considering development of biomedical devices for use with humans and especially the elderly or people with disabilities it is important to consider that the device not only is safe, but it feels safe for the user and if relevant for the person aiding the patient. One way of achieving this is having sit-down movement slow down at the end or making sure that the force action on another person is below a certain threshold.

As shown in Pchelkin et al. (2014) once a control system has been found for a system it turns out that one really has found a control system for a family of different systems with great robustness for uncertainties in parameters or the environment the robot is acting.

1.2 Scope

It became clear during work on the project that working with a system with $n = 3$ degrees of freedom was to complicated to work with at this time.

Therefore the project will be simplified to work with a cart-pendulum system rather than a humanoid robot with more degrees of freedom. The plan is to further study this in the master thesis project.

1.3 Tasks

1. Perform a study on theory of underactuated systems
2. Investigate desirable characteristics of sit-down motions
3. Simulate an underactuated system and find a controller which achieves the desired motion
4. Discuss relevance for more degrees of freedom

1.4 Structure

First a literature review will be presented. Furthermore general theory will be reviewed, the results of the simulation will be shown and analysed before discussion and concluding remarks.

Chapter 2

Literature Review

2.1 Underactuated systems

Over the last decade and a half there has been developed methods of stabilizing underactuated mechanical systems for a given orbit using Virtual holonomic constraints(VHC) for instance in Shiriaev et al. (2005).

The method is powerful because it can be applied to various different mechanical systems as shown the previous mentioned paper, but also in more complicated systems as in Mettin et al. (2008) and Pchelkin et al. (2014) Where they use this method to plan and control more human-like movements of humanoid robots with $n = 3$ or more degrees of freedom .

2.2 Humanoid Robots

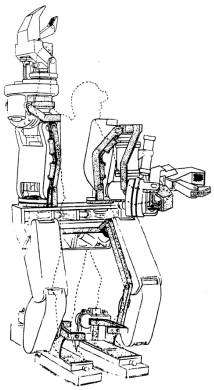

Figure 2.1: Hardiman I prototype, GENERAL ELECTRIC CO SCHENECTADY NY SPECIALTY MATERIALS HANDLING PRODUCTS OPERATION, Public domain, via Wikimedia Commons(Fick and Makinson, 2012)

Starting with General Electrics "Hardiman I" worked on from 1965-1971(GE, 2016) shown in figure 2.1 there has been attempts to construct devices/exoskeletons for use in human rehabilitation or augmentation. There is increasing interest in developing these technologies and there has been great strides on the hardware front, but these devices often lack sophisticated control methods or rely on supports like crutches(for instance Ekso Bionics EksoNR(Ekso Bionics, 2021)). There has also been some research on hands-free/support free walking as in (Harib et al., 2018). Here the authors specifically cite the need for control algorithms that addresses model uncertainties, a strength of orbital stabilization via transverse linearization as will be attempted here.

A question that arises in control of humanoid robots is what characterises an optimal movement of such a robot/device? For instance humans and other animals use their spring-like muscle to conserve energy during walking or running(control of such a system is achieved in (Mettin et al., 2009) in other situations there might be other goals like soft landing or small forces(Normal forces, N or forces acting on other agents like people aiding in rehabilitation of a patient or aiding the patient in the movement itself).

Chapter 3

Basic Theory

3.1 Underactuated systems

In general robot systems can be described by a Euler - Lagrange system like this:

$$M(q)\begin{bmatrix}\ddot{q}_1\\ \ddot{q}_2\\ \vdots\\ \ddot{q}_n\end{bmatrix} + C(q,\dot{q})\begin{bmatrix}\dot{q}_1\\ \dot{q}_2\\ \vdots\\ \dot{q}_n\end{bmatrix} + G(q) = \begin{bmatrix}\tau_1\\ \tau_2\\ \vdots\\ \tau_n\end{bmatrix} \tag{3.1}$$

where $q, \dot{q} \in \mathcal{R}^n$ and τ_i is the generalized external forces.M is the inertia matrix, C is the Coriolis and centrifugal generalized forces and G is the contribution of potential energy due to gravity. When a system is underactuated one or more of these τ_i will be 0, meaning we have no way of influencing that joint directly by control action.

3.2 System dynamics

If we consider a point mass m at distance l from a suspension point attached to a cart with mass M. The rod is assumed mass-less. The acceleration due to gravity is g. The cart can move on the horizontal and one can apply a force f to move it, see figure 3.1.

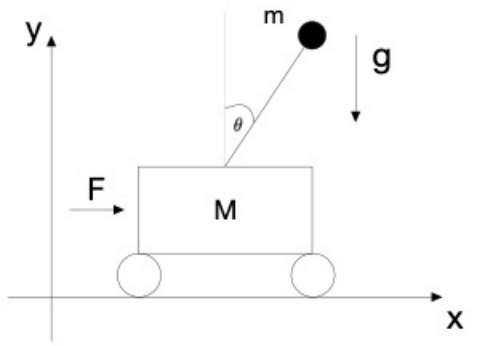

Figure 3.1: A cart of mass M, with a point-mass, m. The pendulum makes an angle θ with the vertical axis

The velocities of the cart and pendulum can be described as:

$$v_1^2 = \dot{x}^2 \tag{3.2}$$

$$v_2^2 = \left(\frac{d}{dt}(x + l \cdot sin(\theta))\right)^2 + \left(\frac{d}{dt}(l \cdot cos(\theta))\right) = \dot{x}^2 + 2\dot{x}\dot{\theta}l \cdot cos(\theta) + l^2\dot{\theta}^2 \tag{3.3}$$

Where v_1 is the velocity of the cart and v_2 the velocity of the point-mass. The kinetic energy of the system of the system is:

$$\mathcal{K} = \frac{1}{2}Mv_1^2 + \frac{1}{2}mv_2^2 = \frac{1}{2}(M+m)\dot{x}^2 + m\dot{x}\dot{\theta}l \cdot cos(\theta) + \frac{1}{2}ml^2\dot{\theta}^2 \tag{3.4}$$

The potential energy is:

$$\mathcal{P} = mgh = mgl \cdot cos(\theta) \tag{3.5}$$

The Lagrangian of the system is:

$$\mathcal{L} = \mathcal{K} - \mathcal{P} = \frac{1}{2}(M+m)\dot{x}^2 + m\dot{x}\dot{\theta}l \cdot cos(\theta) + \frac{1}{2}ml^2\dot{\theta}^2 - mgl \cdot cos(\theta) \tag{3.6}$$

The Lagrangian equations are then:

$$\frac{d}{dt}\frac{\partial \mathcal{L}}{\partial \dot{x}} - \frac{\partial \mathcal{L}}{\partial x} = (M+m)\ddot{x} + m\ddot{\theta}l \cdot cos(\theta) - ml \cdot sin(\theta)\dot{\theta}^2 = f \tag{3.7}$$

$$\frac{d}{dt}\frac{\partial \mathcal{L}}{\partial \dot{\theta}} - \frac{\partial \mathcal{L}}{\partial \theta} = m\ddot{x}l \cdot cos(\theta) + ml^2\ddot{\theta} - mgl \cdot sin(\theta) \tag{3.8}$$

After some algebraic manipulation the final equations of motion are found in (3.9):

$$\begin{aligned} &(m+M) \cdot \ddot{x} + cos(\theta) \cdot m\ddot{\theta}l - ml \cdot sin(\theta)\dot{\theta}^2 = f \\ &cos(\theta) \cdot \ddot{x} + l\ddot{\theta} - g \cdot sin(\theta) = 0 \end{aligned} \tag{3.9}$$

In matrix form this can be re-written as:

$$\begin{bmatrix} (m+M) & cos(\theta) \cdot ml \\ cos(\theta) & l \end{bmatrix} \begin{bmatrix} \ddot{x} \\ \ddot{\theta} \end{bmatrix} = \begin{bmatrix} ml \cdot sin(\theta)\dot{\theta}^2 \\ g \cdot sin(\theta) \end{bmatrix} + \begin{bmatrix} 1 \\ 0 \end{bmatrix} f \tag{3.10}$$

By some manipulations this becomes:

$$\begin{bmatrix} \ddot{x} \\ \ddot{\theta} \end{bmatrix} = F(\theta, \dot{\theta}) + G(\theta) \cdot f \tag{3.11}$$

$$F(\theta, \dot{\theta}) = \frac{1}{(m+M) \cdot l - cos^2(\theta) \cdot ml} \begin{bmatrix} l & -cos(\theta) \cdot ml \\ -cos(\theta) & (m+M) \end{bmatrix} \cdot \begin{bmatrix} ml \cdot sin(\theta) \cdot \dot{\theta}^2 \\ g \cdot sin(\theta) \end{bmatrix} = \begin{bmatrix} f_1 \\ f_2 \end{bmatrix} \tag{3.12}$$

$$G(\theta) = \frac{1}{(m+M) \cdot l - cos^2(\theta) \cdot ml} \begin{bmatrix} l \\ -cos(\theta) \end{bmatrix} = \begin{bmatrix} g_1 \\ g_2 \end{bmatrix} \tag{3.13}$$

3.3 Motion Generator

It is desired that the angle θ is chosen as the motion generator. Such that a desired path θ^* gives the motion of the entire system.

Let $x = \phi(\theta^*)$ then the passive equation becomes:

$$\begin{gathered} cos(\theta) \left[\phi'(\theta)\ddot{\theta} + \phi''(\theta)\dot{\theta}^2) \right] + l\ddot{\theta} - g \cdot sin(\theta) = \\ \left[l + cos(\theta)\phi'(\theta) \right] \ddot{\theta} + cos(\theta)\phi''(\theta)\dot{\theta}^2 - g \cdot sin(\theta) = 0 \end{gathered} \tag{3.14}$$

This becomes the $\alpha - \beta - \gamma$-equation for the problem

$$\alpha(\theta)\ddot{\theta} + \beta(\theta)\dot{\theta}^2 + \gamma(\theta) = 0 \tag{3.15}$$

$$\dot{x} = \phi'(\theta^*)\dot{\theta^*} \tag{3.16}$$

$$\ddot{x} = \phi''(\theta^*)\dot{\theta^*}^2 + \phi'(\theta^*)\ddot{\theta^*} \tag{3.17}$$

For a synchronization function a polynomial in θ of degree 3 is chosen

$$\phi(\theta) = k_0 + k_1\theta + k_2\theta^2 + k_3\theta^3 \tag{3.18}$$

$$\phi'(\theta) = k_1 + 2k_2\theta + 3k_3\theta^2 \tag{3.19}$$

$$\phi''(\theta) = 2(k_2 + 3k_3\theta) \tag{3.20}$$

$$\ddot{\theta} = \frac{g \cdot sin(\theta) - \dot{\theta}^2 cos(\theta)\phi''(\theta)}{l + cos(\theta) \cdot \phi'(\theta)} = \frac{g \cdot sin(\theta) - \dot{\theta}^2 cos(\theta) \cdot 2(k_2 + 3k_3\theta)}{l + cos(\theta) \cdot (k_1 + 2k_2\theta + 3k_3\theta^2)} \tag{3.21}$$

The system has an equilibrium at $\theta_e = 0$, for it to have a center the linerization of the $\alpha\beta\gamma$-representation of the system(3.22).

$$\ddot{z} + \left[\frac{d}{d\theta} \frac{\gamma(\theta)}{\alpha(\theta)} \right] |_{\theta=0} \cdot z = 0 \tag{3.22}$$

must also have a center at zero $\rightarrow \frac{\gamma(\theta)}{\alpha(\theta)}|_{\theta=0} = 0$, $\frac{\beta(\theta)}{\alpha(\theta)}|_{\theta=0} \neq \pm\infty$ and:

$$\left[\frac{d}{d\theta}\frac{\gamma(\theta)}{\alpha(\theta)}\right]|_{\theta=0} > 0 \rightarrow \frac{-g \cdot cos(\theta)}{l + cos(\theta)\phi'(\theta)}|_{\theta=0} = \frac{-g}{l+k_1} > 0 \rightarrow k_1^* < -l. \tag{3.23}$$

The total energy of the system written in the θ-parametrization is:

$$\begin{aligned} &E(\theta, \dot{\theta}) = \\ &\frac{1}{2}(m+M)\dot{\theta}^2(k_1 + 2k_2\theta + 3k_3\theta^2)^2 \\ &+ ml\dot{\theta}^2(k_1 + 2k_2\theta + 3k_3\theta^2) \cdot cos(\theta) + \frac{1}{2}ml^2\dot{\theta}^2 + mgl \cdot cos(\theta) \end{aligned} \tag{3.24}$$

3.4 Transverse Linearization

Our goal is now to find a transverse linerarization with the form:

$$\begin{aligned} \dot{I}_* &= a_{11}(t)I_* + a_{12}(t)y_* + a_{13}(t)\dot{y}_* + b_1(t)v_* \\ \ddot{y}_* &= v \end{aligned} \tag{3.25}$$

The origin of this linearized system can then be stabilized by $v(t) = K(t)x_\perp$ as defined in (3.39).

The functions of $\left[\theta, x, \dot{\theta}, \dot{x}\right]$ that define the three needed transverse coordinates for the desired motion are:

$$\begin{aligned} x_{1_\perp} &= y = x - \phi(\theta) \\ x_{2_\perp} &= \dot{y} = \dot{x} - \phi'(\theta)\dot{\theta} \\ x_{3_\perp} &= I = \dot{\theta}^2 - exp\left\{-2\int_{\theta_0}^{\theta}\frac{\beta(\tau)}{\alpha(\tau)}d\tau\right\}\left[(\dot{\theta}_0^2) - exp\left\{-2\int_{\theta_0}^{s}\frac{\beta(\tau)}{\alpha(\tau)}d\tau\right\}\frac{2\gamma(s)}{\alpha(s)}ds\right] \end{aligned} \tag{3.26}$$

Where $\alpha(s) = l + cos(s) \cdot \phi'(s)$,$\beta(s) = cos(s) \cdot \phi''(s)$ and $\gamma(s) = -g \cdot sin(s)$

The linearization of the transverse dynamics are found by using the equations of motions(3.9) and write them in in new variables $[\theta, y]$ with the new control input v. With $y = x - \phi(\theta)$, the relation in (3.27)

$$\ddot{y} = \ddot{x} - \phi''(\theta)\dot{\theta}^2 - \phi'(\theta)\ddot{\theta} \tag{3.27}$$

The next step is to find functions

$$g_y(\theta, \dot{\theta}, y, \dot{y}) \tag{3.28}$$

$$g_{\dot{y}}(\theta, \dot{\theta}, y, \dot{y}) \tag{3.29}$$

$$g_v(\theta, \dot{\theta}, y, \dot{y}) \tag{3.30}$$

such that:

$$\begin{aligned}\alpha(\theta)\ddot{\theta} + \beta(\theta)\dot{\theta}^2 + \gamma(\theta) &= g_y(\theta,\dot{\theta},y,\dot{y})y + g_{\dot{y}}(\theta,\dot{\theta},y,\dot{y})\dot{y} + g_v(\theta,\dot{\theta},y,\dot{y})v \\ \ddot{y} &= v\end{aligned} \tag{3.31}$$

From (3.27) we can insert the expression for $\ddot{x}$ into the passive dynamics (3.9) this leads to:

$$\begin{aligned}&\left[l + cos(\theta)\phi'(\theta)\right]\ddot{\theta} + cos(\theta)\phi''(\theta)\dot{\theta}^2 - g \cdot sin(\theta) \\ =&\alpha(\theta)\ddot{\theta} + \beta(\theta)\dot{\theta}^2 + \gamma(\theta) = -cos(\theta)\cdot\ddot{y} = g_v(\theta,\dot{\theta},y,\dot{y})\cdot v\end{aligned} \tag{3.32}$$

The system in (3.25) can now be written as:

$$\frac{d}{dt}\begin{bmatrix} I \\ y \\ \dot{y}\end{bmatrix} = \begin{bmatrix} a_{11}(t) & a_{12}(t) & a_{13}(t) \\ 0 & 0 & 1 \\ 0 & 0 & 0\end{bmatrix}\begin{bmatrix} I \\ y \\ \dot{y}\end{bmatrix} + \begin{bmatrix} b_1(t) \\ 0 \\ 1\end{bmatrix} v = A(t)x_\perp + B(t)v \tag{3.33}$$

in our case $a_{12} = a_{13} = 0$ and

$$\begin{aligned}a_{11}(t) &= -\frac{2\dot{\theta}^*(t)\cdot\beta(\theta^*(t))}{\alpha(\theta^*(t))} = -\frac{2\dot{\theta}^*(t)\cdot cos(\theta^*(t))\cdot\phi''(\theta^*(t))}{l + cos(\theta^*(t))\phi'(\theta^*(t))} \\ b_1(t) &= \frac{2\dot{\theta}^*(t)\cdot g_v(t)}{\alpha(\theta^*(t))} = -\frac{2\dot{\theta}^*(t)\cdot cos(\theta^*(t))}{l + cos(\theta^*(t))\phi'(\theta^*(t))}\end{aligned} \tag{3.34}$$

Using the equations of motions one must then find a feedback transformation $v \to f$, the feedback transformation can be found in (3.36).

Using the simplified dynamics in (3.12) and (3.13) along with (3.27) we have:

$$v = \ddot{y} = f_1(\theta,\dot{\theta}) + g_1(\theta)\cdot f - \phi''(\theta)\dot{\theta}^2 - \phi'(\theta)\cdot(f_2(\theta,\dot{\theta}) + g_2(\theta)\cdot f) \tag{3.35}$$

and by algebraic manipulations:

$$f = \frac{v - (f_1(\theta,\dot{\theta}) - f_2(\theta,\dot{\theta})\cdot\phi'(\theta) - \phi''(\theta)\cdot\dot{\theta}^2}{g_1(\theta) - \phi'(\theta)g_2(\theta)} \tag{3.36}$$

3.5 Linear-Quadratic Regulator

To stabilize the origin of the augmented system (3.33) corresponding to the nominal behaviour i.e $y = 0 \to x = \phi(\theta)$, $\dot{y} = 0 \to \dot{x} = \phi'(\theta)\dot{\theta}$ and $I = 0$, one finds the LQR-gain matrix $K(t)$ by solving the matrix Riccatti differential equation with Periodic coefficients(PRDE) (3.38) with (3.37).

$$P(t) = P(t+T) \quad \text{and} \quad P(t) = P(t)^T \quad \text{for all} \quad t \in [0,T] \tag{3.37}$$

and

$$\dot{P}(t) + A(t)^T P(T) + P(t)A(t) + Q = P(t)B(t)R^{-1}B(t)^T P(t) \quad \forall t \in [0,T]. \tag{3.38}$$

Where Q and R are constant weights on the state and control input respectively, $A(t)$ and $B(t)$ are as defined in (3.33). This equation can then be solved numerically as shown in (Shiriaev et al., 2005). This leads to the expression for K in (3.39)

$$K(t) = -R^{-1}B(t)^T P(t) \tag{3.39}$$

This $K(t)$ minimizes the quadratic cost function:

$$J = \int_0^\infty \left[x(t)^T Q(t)x(t) + u(t)^T R(t)u(t)\right]\, dt \tag{3.40}$$

wrt. $u(t)$ on solutions of the periodic system:

$$\dot{x}(t) = A(t)x(t) + B(t)u(t), \quad x(0) = x_0 \tag{3.41}$$

(3.40) and (3.41) as presented in (Gusev et al., 2010)

Chapter 4

Experiment

For simplicity the mass of the cart M, the mass of the pendulum m and the length of the rod l is set at 1.

Parameter	Pendulum	Cart
length(m)	1	-
Mass(kg)	1	1
Gravitational constant(m/s^2)	9.81	-

Table 4.1: Experimental Parameters

The goal is to stabilize one of the orbits in phase plot seen in 4.1 As seen in figure 4.1 there clearly is a center at $\theta = \dot{\theta} = 0$.

The Pendulum on a cart system was simulated using MATLAB(MATLAB, 2020) with the parameters found in table 4.1, with boundary conditions in table 4.2 an the coefficients of the synchronization function in table 4.3.

Initial Conditions	Pendulum($\theta, \dot{\theta}$)	Cart($x, \dot{x}$)
	(0.6,-0.3)	(0.2,-0.2)
End Conditions		
	($\frac{\pi}{2}$,0.5)	-

Table 4.2: Boundary Conditions

The coefficients k_i(table 4.3) were found using the initial conditions and the fact that $x_0 = k_0 + k_1\theta + k_2\theta^2 + k_3\theta^3$, $\dot{x}_0 = k_1\dot{\theta} + 2k_2\dot{\theta}\theta + 3k_3\dot{\theta}\theta^2$ and that the energy function (3.24) is constant on the motion. The most promising trajectory is shown in figure 4.2 some other trajectories can be found in the appendix.

Was not able to find a solution to the PRDE(3.41) and hence not able to control the feedback linearised system.

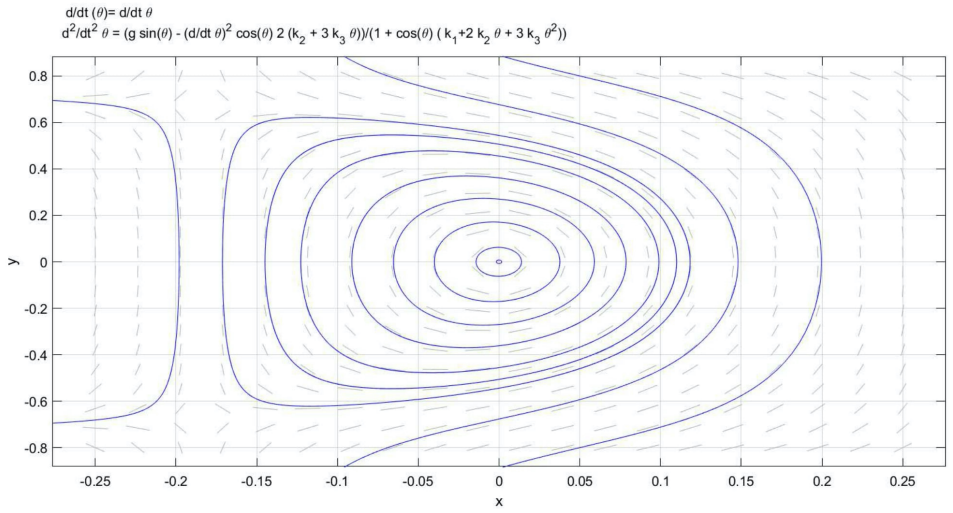

Figure 4.1: Phase plot for the $\alpha\beta\gamma$-system

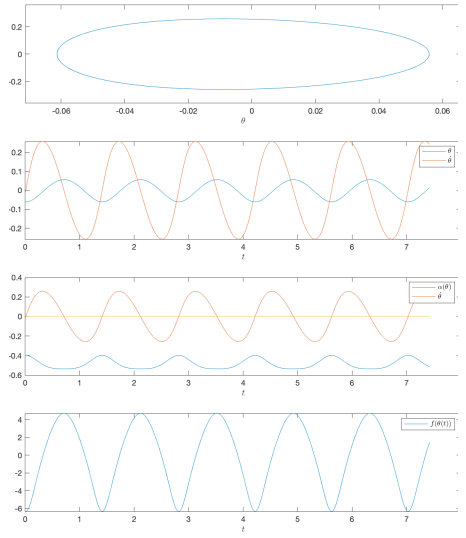

Figure 4.2: The most promising solution $\theta^*(t)$ with phase portrait, $\alpha(\theta)$ plotted with $\dot{\theta^*}(t)$ and the force($f(\theta(t))$) applied to the cart to have that trajectory.

k_i	Value
k_0	0.73468
k_1	-1.5
k_2	-0.5668
k_3	2.63595

Table 4.3: Coefficients for the synchronization function $\phi(\theta)$.

Chapter 5

Analysis

5.1 Results

As can be seen in figure 4.2 a promising trajectory was found, with this trajectory it seems possible to stabilize the system at $\frac{\pi}{2}$. However a solution to the PRDE was not found and without that periodic LQR-gain K(t) the linear feedback system (3.33) wasn't stabilized at the origin. Solving the PRDE is a non-trivial task and further study on the subject is required by the author.

5.2 Sources of error

It bears mentioning that Pplane(Harvey, 2018) which was used for drawing these phase portraits has not been optimized for MATLAB R2020/b. There was several minor errors during the drawing of these phase portraits.

The project has also shown the lack of robustness in using Simulink's(Documentation, 2020) blocks for simulating such a complicated system. Simulink blocks provide perspective on the systems and makes it easier to do a modular approach where the system is built piece by piece, but one spends a lot of time checking signals, dimensions of matrices and so on.

5.3 Potential improvements

The challenge in Orbital Stabilization of underactuated systems comes not in the methods itself because they are quite intuitive, but in finding good synchronization functions, $\phi(\theta)$, periodic trajectories,$\theta^*(t)$ for the system and solving the PRDE is also a challenge that must be overcome.

It is also important to have some knowledge of the system to be stabilized. In hindsight it seems obvious that stable oscillations around the horizontal is a challenge. Because if one wants to have a constant angle of the pendulum near the horizontal, the cart must

accelerate. But in that case the system will no longer be periodic in x. (Surov et al., 2017) presents a novel approach not for handling or avoiding such singularities, but as an opportunity to find new periodic trajectories.

The trajectories shown in figure 4.2 and the appendix avoided this singularity. It is also possible to avoid these issues if $\alpha(\theta) = 0$ only where $\dot{\theta}$ also is zero Other minor improvements is finding better tools for simulating systems and drawing phase portraits. Mainly simulating directly in MATLAB and find another tool than pplane to draw the phase portraits.

Chapter 6

Conclusion

> Ever tried. Ever failed. No matter. Try again. Fail again. Fail better.(Beckett, 1983)

Looking back on the task enumerated in 1.3.There was a lot that wasn't achieved. This was disappointing, but a lot was learned and hopefully the things learned throughout the semester will have time to mature before the master thesis project.

Although the simulations failed this is not an indictment of the methods itself. The challenge for the engineer is to understand the model of the system in question, find periodic trajectories, good synchronization functions and then solving the PRDE. Once this things are achieved they have powerful tools in their toolbox in the form of Orbital Stabilization, Transverse linearization and feedback control.

6.1 Future work and continuation

For the masters thesis which will be about adjacent topics the work on this project has shown the holes in the authors knowledge on the subject. So further research in the field is required before one can take further steps. Thankfully it seems that the field has furtive ground for research and a lot of different approaches are taken, both in specific systems and in the development of more general approaches. So opportunities for learning are plentiful.

Firstly familiarization with methods for solving PRDE is required, there has been a lot of work on different ways of doing this, for instance in Gusev et al. (2016) and in (Gusev et al., 2010) there is a evaluation of several different methods. The next step is to expand this approach to a more general robotic system with more degrees of freedom(at least n=3 or 4), a question to be asked in that regard is how many degrees of freedom are necessary to describe the sit-down/rise motion of a human? This is investigated somewhat in Pchelkin et al. (2014), but it could be relevant to investigate this further. It would also be interesting to test the control method on existing technology for assisting rising/sitting motion. Where control methods can be improved upon.

Bibliography

Asimov, I., 2008. I, Robot. Bantam Spectra.

Beckett, S., 1983. Worstward ho. Grove Pr.

Documentation, S., 2020. Simulation and model-based design. URL: https://www.mathworks.com/products/simulink.html.

Ekso Bionics, 2021. EksoNR - the next step in NeuroRehabilitation. https://eksobionics.com/eksonr/. Accessed: 2021-12-15.

Fick, B.R., Makinson, J.B., 2012. Hardiman I Prototype. URL: https://upload.wikimedia.org/wikipedia/commons/5/50/Hardiman_I.png.

GE, 2016. Do you even lift, bro? Hardiman was GE's muscular take on the human-machine interface. https://www.ge.com/news/reports/do-you-even-lift-bro-hardiman-and-the-human-machine-interface. Accessed: 2021-12-15.

Gusev, S., Johansson, S., Kågström, B., Shiriaev, A., Varga, A., 2010. A numerical evaluation of solvers for the periodic riccati differential equation. BIT Numerical Mathematics 50, 301–329. doi:10.1007/s10543-010-0257-5.

Gusev, S.V., Shiriaev, A.S., Freidovich, L.B., 2016. Sdp-based approximation of stabilising solutions for periodic matrix riccati differential equations. International Journal of Control 89, 1396–1405. doi:10.1080/00207179.2015.1131850.

Harib, O., Hereid, A., Agrawal, A., Gurriet, T., Finet, S., Boeris, G., Duburcq, A., Mungai, M.E., Masselin, M., Ames, A.D., et al., 2018. Feedback control of an exoskeleton for paraplegics: Toward robustly stable, hands-free dynamic walking. IEEE Control Systems 38, 61–87. doi:10.1109/mcs.2018.2866604.

Harvey, H., 2018. Pplane. URL: https://www.mathworks.com/matlabcentral/fileexchange/61636-pplane. MATLAB Central File Exchange. Retrieved December 16, 2021.

MATLAB, 2020. version 9.9.0.1718557 (R2020b). The MathWorks Inc., Natick, Massachusetts.

Mettin, U., Hera, P.X.L., Freidovich, L.B., Shiriaev, A.S., 2009. Parallel elastic actuators as a control tool for preplanned trajectories of underactuated mechanical systems. The International Journal of Robotics Research 29, 1186–1198. doi:10.1177/0278364909344002.

Mettin, U., Hera, P.X.L., Freidovich, L.B., Shiriaev, A.S., Helbo, J., 2008. Motion planning for humanoid robots based on virtual constraints extracted from recorded human movements. Intelligent Service Robotics 1, 289–301. doi:10.1007/s11370-008-0027-2.

Pchelkin, S., Shiriaev, A.S., Freidovich, L.B., Mettin, U., Gusev, S.V., Kwon, W., Paramonov, L., 2014. A dynamic human motion: coordination analysis. Biological Cybernetics 109, 47–62. doi:10.1007/s00422-014-0624-4.

Shiriaev, A., Perram, J., Canudas-De-Wit, C., 2005. Constructive tool for orbital stabilization of underactuated nonlinear systems: virtual constraints approach. IEEE Transactions on Automatic Control 50, 1164–1176. doi:10.1109/tac.2005.852568.

Surov, M.O., Gusev, S.V., Shiriaev, A.S., 2017. Shaping stable oscillation of a pendulum on a cart around the horizontal. IFAC-PapersOnLine 50, 7621–7626. doi:10.1016/j.ifacol.2017.08.1146.

Appendix

Trajectories

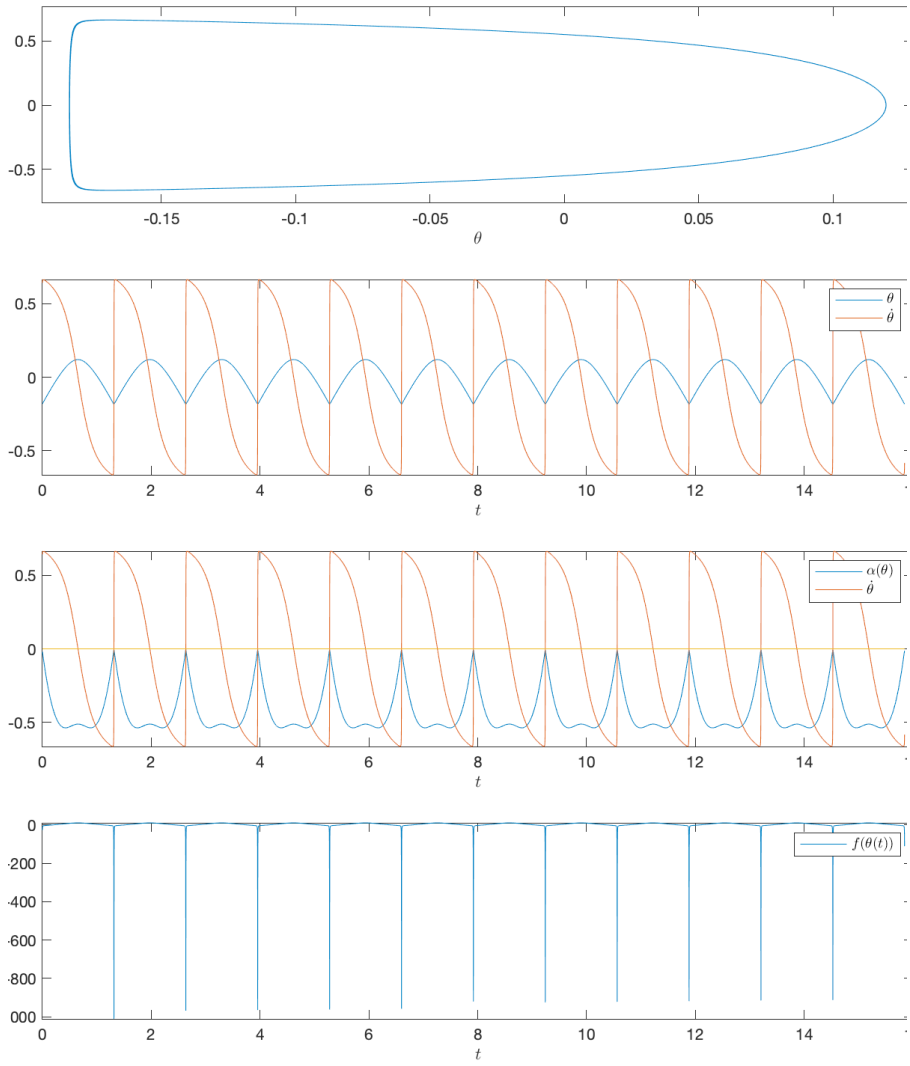

Figure 6.1: A: A solution $\theta^*(t)$ with phase portrait, $\alpha(\theta)$ plotted with $\dot{\theta^*}(t)$ and the force($f(\theta(t))$) applied to the cart to have that trajectory.

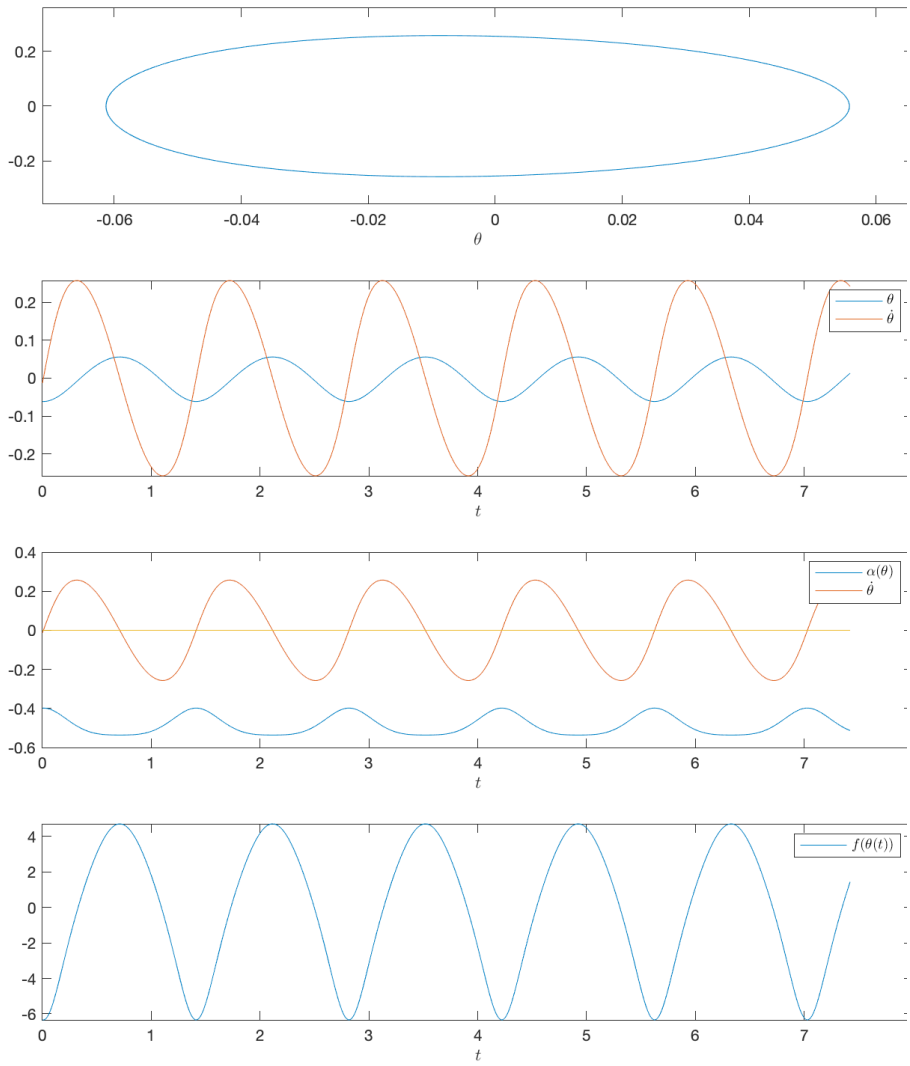

Figure 6.2: The most promising solution $\theta^*(t)$ with phase portrait, $\alpha(\theta)$ plotted with $\dot{\theta^*}(t)$ and the force($f(\theta(t))$) applied to the cart to have that trajectory.

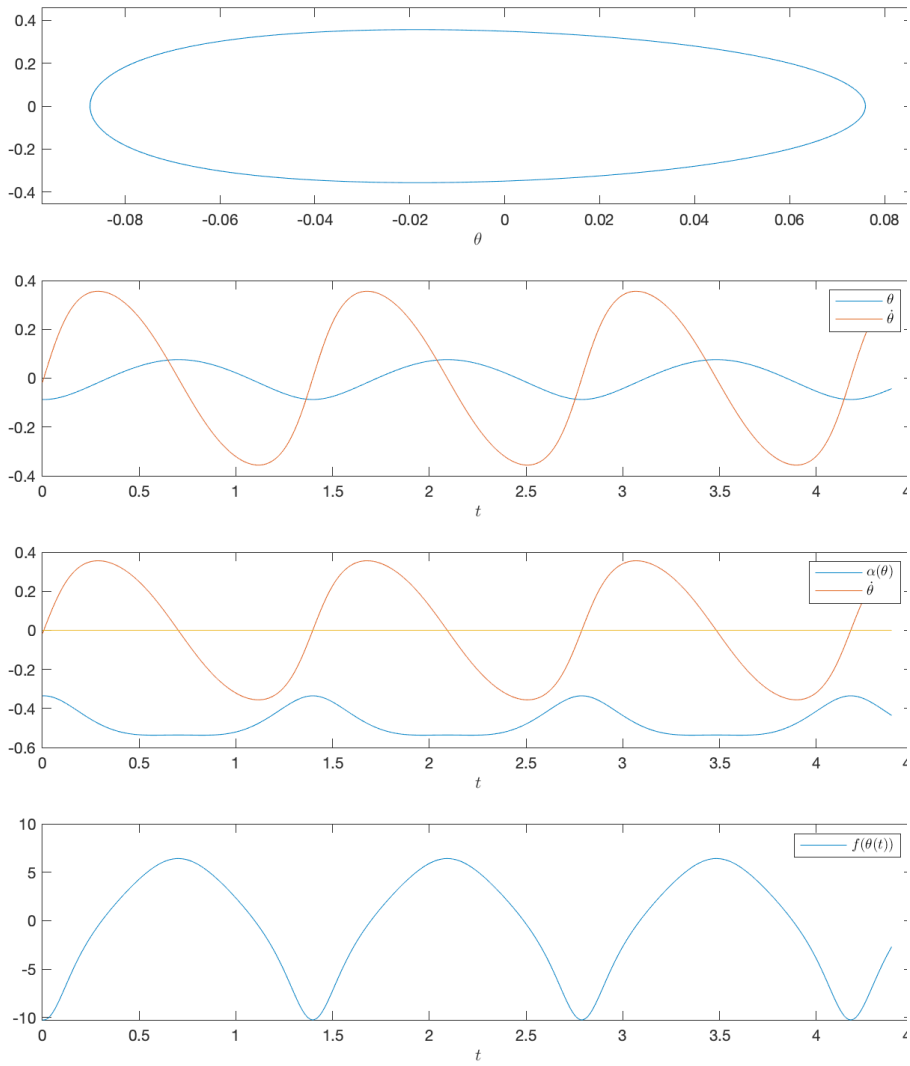

Figure 6.3: B: A solution $\theta^*(t)$ with phase portrait, $\alpha(\theta)$ plotted with $\dot{\theta^*}(t)$ and the force($f(\theta(t))$) applied to the cart to have that trajectory.

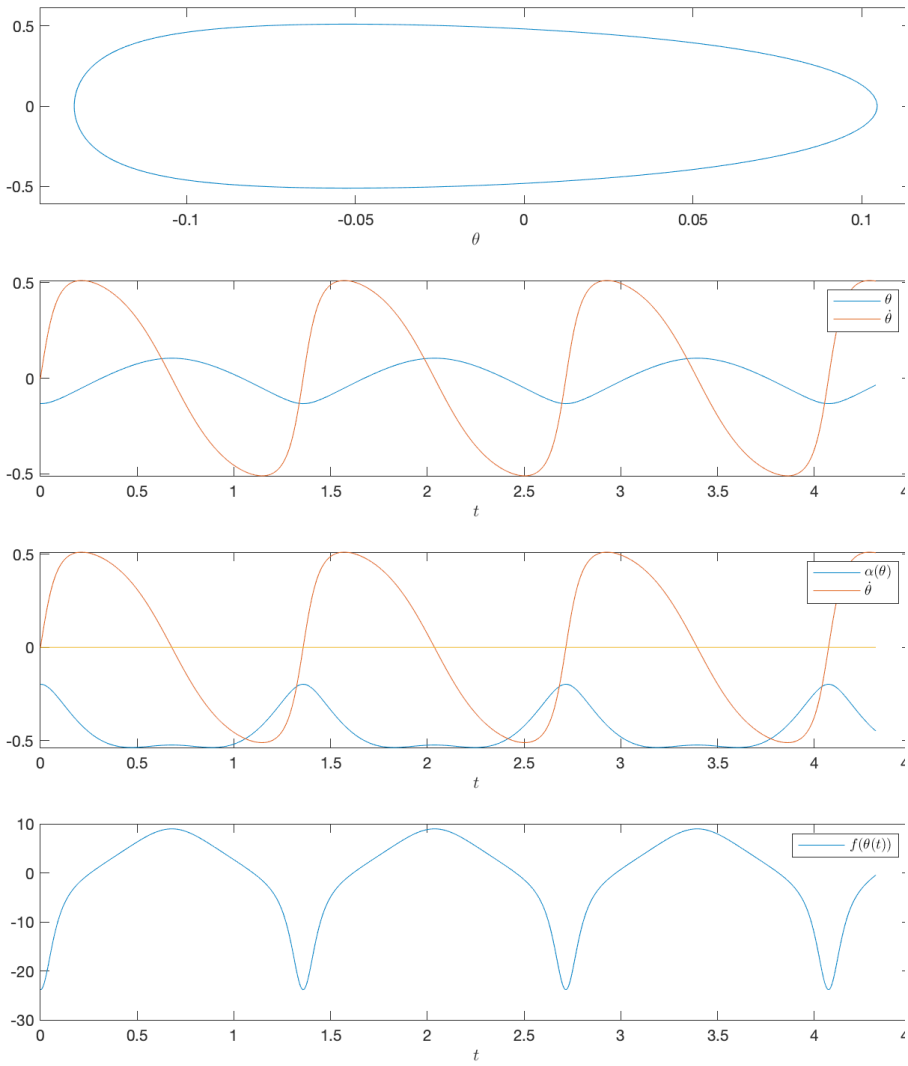

Figure 6.4: C: A solution $\theta^*(t)$ with phase portrait, $\alpha(\theta)$ plotted with $\dot{\theta^*}(t)$ and the force($f(\theta(t))$) applied to the cart to have that trajectory.

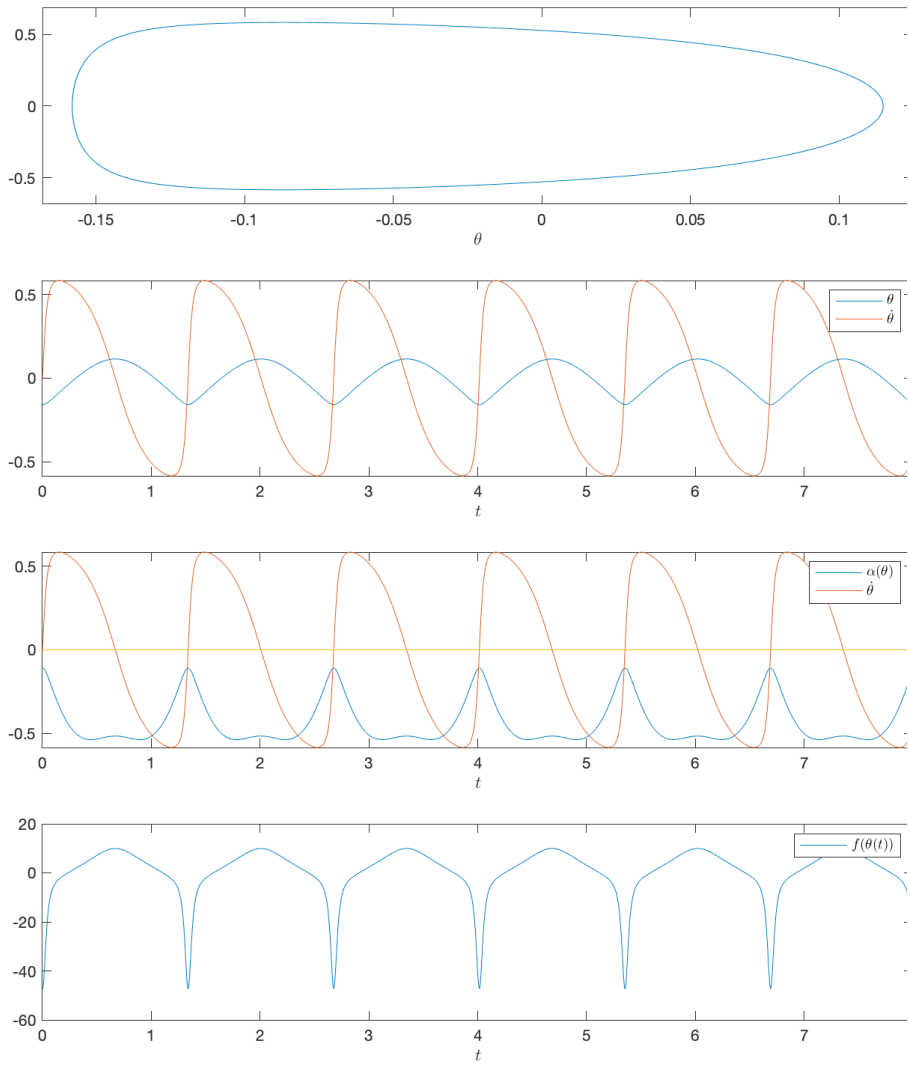

Figure 6.5: D: A solution $\theta^*(t)$ with phase portrait, $\alpha(\theta)$ plotted with $\dot{\theta^*}(t)$ and the force($f(\theta(t))$) applied to the cart to have that trajectory.

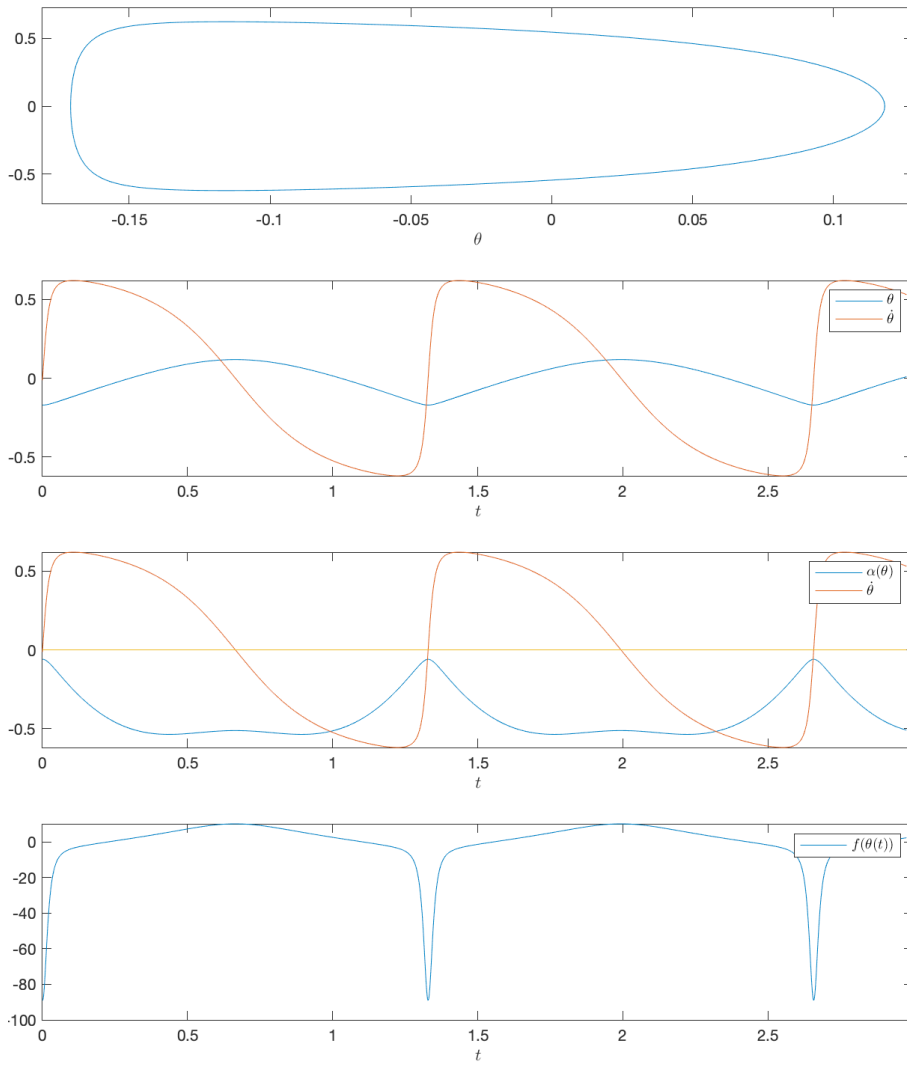

Figure 6.6: E: A solution $\theta^*(t)$ with phase portrait, $\alpha(\theta)$ plotted with $\dot{\theta^*}(t)$ and the force($f(\theta(t))$) applied to the cart to have that trajectory.

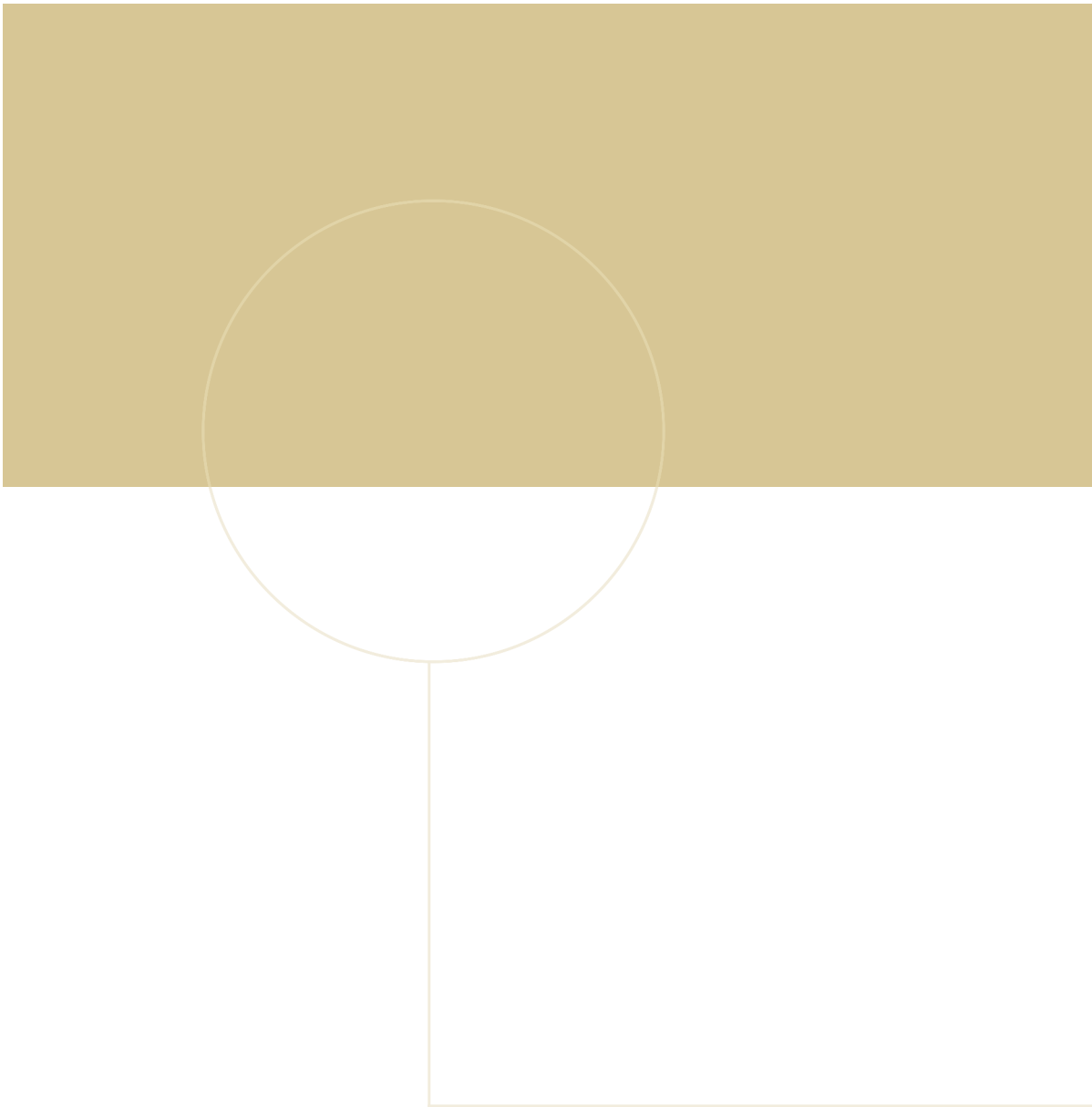

NTNU

Norwegian University of
Science and Technology